Miocene to Holocene marine tephrostratigraphy offshore northern Central America and southern Mexico: Pulsed activity of known volcanic complexes

Schindlbeck, J.C.[1], Kutterolf, S.[2], Freundt, A.[2], Eisele, S.[3], Wang, K.-L.[4,5], Frische, M.[2]

[1]Heidelberg University, Institute of Earth Sciences, Im Neuenheimer Feld 234-236, 69120 Heidelberg, Germany

[2]GEOMAR Helmholtz Centre for Ocean Research Kiel, 24148 Kiel, Germany

[3] Asian School of the Environment, Nanyang Technological University, Singapore

[4]Institute of Earth Sciences, Academia Sinica, Taipei 11529, Taiwan

[5]Department of Geosciences, National Taiwan University, Taipei 106, Taiwan

Corresponding author: Julie C. Schindlbeck (Julie.Schindlbeck@geow.uni-heidelberg.de)

Key Points:

- Stratigraphically classified tephra database of glass compositions with correlations of marine and terrestrial tephra layers
- New insights into the lifetime of the major volcanic centers in Guatemala and El Salvador and their number of major eruptions
- Identification of five pulses of enhanced volcanic activity during the Quaternary, the Pliocene, the Late, Middle Miocene and Early

This article has been accepted for publication and undergone full peer review but has not been through the copyediting, typesetting, pagination and proofreading process which may lead to differences between this version and the Version of Record. Please cite this article as doi: 10.1029/2018GC007832

Abstract

We studied the tephra inventory of fourteen deep sea drill sites of three DSDP and ODP legs drilled offshore Guatemala and El Salvador (Legs 67, 84, 138), and one leg offshore Mexico (Leg 66). Marine tephra layers reach back from the Miocene to the Holocene. We identified 223 primary ash beds and correlated these between the drill sites, with regions along the volcanic arcs, and to specific eruptions known from land. In total, 24 correlations were established between marine tephra layers and to well-known Quaternary eruptions from El Salvador and Guatemala. Additional 25 tephra layers were correlated between marine sites. Another 108 single ash layers have been assigned to source areas on land resulting in a total of 157 single eruptive events. Tephra layer correlations to independently dated terrestrial deposits provide new time markers and help to improve or confirm age models of the respective drill sites. Applying the respective sedimentation rates derived from the age models, we calculated ages for all marine ash beds. Hence, we also obtained new age estimates for eight known, but so far undated large terrestrial eruptions. Furthermore, this enables us to study the temporal evolution of explosive eruptions along the arc and we discovered five pulses of increased activity: 1) a pulse during the Quaternary, 2) a Pliocene pulse between 6 and 3 Ma, 3) a Late Miocene pulse between 10 and 7 Ma, 4) a Middle Miocene pulse between 17–11 Ma, and 5) an Early Miocene pulse (~>21 Ma).

1 Introduction

Understanding the long-term evolution of volcanic systems is one important way of assessing future volcanic hazards (e.g., Freundt et al., 2006; Kutterolf et al., 2013). This is especially important for regions along volcanic arcs that are highly populated and therefore particularly vulnerable in case of a natural catastrophe. Highly explosive volcanism is an essential part of the arc volcanism particularly in ocean-continent subduction zones and is assumed to be representative for the entire arc volcanism in these regions (e.g., Pyle 1995; Mason et al., 2004; Deligne et al., 2010). Widely distributed ash, as one major eruptive product, is best preserved in mostly non-erosive marine and lacustrine environments, which thus provide the most complete record of such highly explosive volcanic activity over long time scales (Keller et al., 1978; Ledbetter, 1985; Carey, 2000; Carey and Sigurdsson, 2000; Kutterolf et al., 2008a; Schindlbeck et al., 2016a,b,c). Wide areal distribution across sedimentary facies boundaries, near-instantaneous emplacement, unambiguous chemical compositions, and the presence of minerals suitable for radio-isotopic dating make the deposits of volcanic eruptions to excellent stratigraphic marker beds in terrestrial and marine sediments. Furthermore they provide constraints on the temporal evolution of both the volcanic source region and the ash-containing sediment facies (e.g., Kutterolf et al., 2008a,b,c,d, 2016; Ponomareva et al., 2013, 2015, 2017; Schindlbeck et al., 2016a,b,c).

In this contribution we focus on tephrostratigraphic correlations between DSDP (Deep Sea Drilling Project) and ODP (Ocean Drilling Program) sites, and the correlation of marine tephras to volcanic complexes and eruptions from Central America. The investigated DSDP/ODP sites are located in the Pacific Ocean offshore the southernmost end of the Trans-Mexican Volcanic Belt (TMVB; Leg 66 drilled in 1979; Watkins et al., 1981), and offshore the northern Central American Volcanic Arc (CAVA) in Guatemala and El Salvador (Fig. 1, 2; Leg 67 drilled in 1979, Leg 84 drilled in 1982, Leg 138 drilled in 1991; Aubouin et al., 1982; von Huene et al., 1985; Mayer et al., 1992). Both arcs are known for numerous Quaternary Plinian and ignimbrite producing eruptions that generated widely dispersed pumice and ash deposits.

The overarching goal of this contribution is to establish a most complete chronotephrostratigraphy for highly explosive eruptions in this region that reaches back to the Early Miocene offshore Guatemala and El Salvador and back to the Late Miocene offshore Mexico. The results contribute to the discussion how the Late Cenozoic explosive volcanism in northern Central America evolved through time and provide new insights into the longevity of known Pleistocene volcanic centers.

2 Geological background and tephrostratigraphy

The volcanic arcs from Mexico, Guatemala and El Salvador are located above the subduction zones of the Cocos Plate and Rivera Microplate that subduct beneath the Caribbean Plate (convergence rate of 70–90 mm/a (Barckhausen et al., 2001; DeMets, 2001)) and the North American Plate (Figs. 1, 2). The CAVA extends continuously from the Mexican-Guatemalan border over ~1100 km to central Costa Rica parallel to the Middle American Trench (MAT; Fig. 1). The TMVB in Mexico is not parallel to the MAT but extends continuously over 1000 km from West to East away from the trench (Fig. 1). Volcanism in Mexico, south of the TMVB, is discontinuous and limited to isolated fields that are also not parallel to the trench (Mora et al., 2007); these include the Chiapanecan Volcanic Arc (CVA) and the Los Tuxtlas Volcanic Field (LTVF; Ferrari et al., 2012) (Fig. 1). Slightly oblique subduction at both, the Northern Central American (El Salvador and Guatemala) as well as the Mexican arc systems, occurs beneath a thick continental crust (40 km). Both subduction systems are erosional convergent margins resuming in high sedimentation rates due to rapid shortening and deepening depositional systems in the forearc (Clift and Vannucchi, 2004).

Central American Volcanic Arc

Along the CAVA, the slightly oblique subduction causes tectonic segmentation of the arc (DeMets, 2001; Funk et al., 2009) and subduction conditions such as state of hydration of the Cocos Plate and composition of its sediment cover, slap dip angle, and upper-plate crustal thickness and composition vary significantly along the subduction zone (Abers et al., 2003; Plank et al., 2002; Hoernle et al., 2002; Syracuse and Abers, 2006; Carr, 1984). This causes systematic regional variations in geochemical compositions of Quaternary volcanic rocks along the arc, and between arc segments, which have been extensively studied (e.g., Carr, 1984; Carr et al., 1990, 2003, 2007a; Feigenson and Carr, 1986; Feigenson et al., 2004; Hoernle et al., 2008; Patino et al., 1997, 2000; Freundt et al., 2014). Principal variations of major element are Na_2O decreases from Guatemala to Nicaragua and subsequent increase in Central Costa Rica (Carr et al., 1984, 2007a), while FeO varies inversely with Na_2O, which Plank and Langmuir (1988) explain with changes of crustal thickness (high Na_2O and low FeO where the crust is thicker). In Central and NW Costa Rica the volcanic rocks of the last 6 Myr carry the ocean island signature of the subducted Cocos Ridge (e.g., Gazel et al., 2009; Carr et al., 2007a; Schindlbeck et al., 2016b). The Ba/La, Ba/Th and U/Th ratios are highest in Nicaragua and decreases towards Guatemala as well as to Costa Rica, which can be attributed to a higher slab sediment component and high fluid flow (Carr et al., 1990; Cameron et al., 2002). The La/Yb ratio instead shows an inverse variation to Ba/La (Carr et al., 2007a) and is a proxy for the degree of melting (Cameron et al., 2002). High Rb/Hf and Th/Nb ratios in Guatemala and northern El Salvador possibly indicate a crustal melt signature (Heydolph et al., 2012; Hannah et al., 2002; Walker et al., 2007).

In the northern part of the arc, volcanic activity can be dated back to the Eocene (Donelly et al., 1990). During Quaternary and Pliocene to Miocene times large caldera systems in El Salvador/Honduras and Guatemala produced large-magnitude eruptions of highly evolved, silicic magmas (e.g., Weyl, 1980; Rose et al., 1999; Jordan et al., 2007a, b; Reynolds 1980, 1987) and some of these large eruptions contributed also to the marine tephra record offshore the southern CAVA (Kutterolf et al., 2008a; Schindlbeck et al., 2016a,b; Jordan et al., 2006). The stratigraphy of several highly explosive eruptions from e.g., Ilopango, Coatepeque, Ayarza, Amatitlán and Atitlán calderas is quite well known for late Pleistocene times (e.g., Koch and McLean, 1975; Rose et al., 1987, 1999; Kwasnitschka, 2009). But less is known about older eruptions from ancestor volcanic systems. The major tephra deposits for the modern calderas from El Salvador and Guatemala are summarized in Figure 3 and Table 1.

Mexican volcanic arcs

Two major volcanic provinces exist in Mexico during the Cenozoic; the Sierra Madre Occidental (Eocene – Middle Miocene) and the TMVB (Miocene – Recent) (e.g., Verma and Carrasco-Núñez, 2003). The arc of the Sierra Madre Occidental strikes north to northwest and lies north of the east-west trending TMVB (outside the northern bounds of Figs. 1, 2a). The relationship and temporal transition of volcanic activity from the Sierra Madre Occidental to the TMVB are still under discussion, but accompanied by a shift in the predominant volcanic products from evolved ignimbrites and rhyolites to andesitic and basaltic lavas (e.g., Morán-Zenteno et al., 1999; Verma and Carrasco-Núñez, 2003; Ferrari et al., 1999). Lenhardt et al. (2010, 2011) postulate an initial phase of the TMVB retained in the Tepoztlán Formation that reaches back to the Early Miocene.

Volcanism in the TMVB is dominated by calc-alkaline Neogene to Quaternary cones, maars, domes and stratovolcanoes, but several areas with alkaline volcanism exist. Several workers proposed genetic models for the TMVB that vary from the classical subduction model, e.g., a mantle plume (e.g., Márquez et al., 1999; Moore et al., 1994) or continental rifting (Sheth et al., 2000; Verma, 2002), to explain the geochemical variations (a review on the TMVB evolution is provided by Ferrari et al., 2012). Detailed tephrostratigraphic studies have been conducted mainly on Holocene to Late Pleistocene deposits (e.g., Ortega-Guerroro and Newton, 1998; Newton and Metcalfe, 1999), whereas studies of Early Pleistocene and Neogene tephra sequences are rare. Several volcanic complexes have produced large eruptions during the Holocene and the Late Pleistocene. A summary of these eruptions is presented in Table 2.

South of the TVMB the volcanism in the Mexican CVA (Fig. 1) is dominated by dome volcanism and associated phreatomagmatic explosive volcanism (Mora et al., 2007). However, El Chichón Volcano, the youngest edifice of the CVA (Damon and Montesinos, 1978) is also known for historical and Holocene highly explosive Plinian eruptions (Macías et al., 2003; Espindola et al. 2000). Little is known about earlier eruptions, although rocks of the volcano flanks were dated to ~200,000-280,000 years BP by K-Ar techniques (Damon and Montesinos, 1978; Duffield et al., 1984).

The LTVF is located on the Gulf of Mexico coastal plain, ~200 km southeast of the TMVB and consist mainly of scoria cones and maars and four major volcanic edifices (Sieron et al., 2014). Lavas of the LTVF have alkaline compositions, which is part of the debate, whether volcanism is related to subduction of the Cocos plate or to extensional tectonics (e.g., Nelson and González-Caver, 1992; Verma, 2006).

Previous marine studies

Several studies investigated the tephra inventory of DSDP/ODP/IODP drill cores and sediment gravity cores along the Middle American Trench and in the Caribbean Sea (e.g., Cadet et al., 1982a,b; Clift et al., 2005; Kutterolf et al., 2007, 2008a; Ledbetter, 1985; Bowles et al., 1973; Jordan et al., 2006; Schindlbeck et al., 2016a,b,c). Ash beds from the Pacific form a tephrostratigraphic framework of large CAVA and Galápagos eruptions back to the Miocene (Kutterolf et al., 2007, 2008a; Schindlbeck et al., 2015, 2016a), whereas the ODP sites of the Caribbean Sea contain Neogene ash beds originated from source volcanoes at the Lesser Antilles and in Honduras and Nicaragua (Jordan et al., 2007b; Carey & Sigurdsson, 2000; Sigurdsson et al., 2000). So far however, the major and trace element geochemistry of the tephra inventory of the DSDP/ODP sites offshore North Central America and Mexico has not been studied in detail with respect to provenance and correlation to terrestrial deposits.

3 Methods

3.1. Sampling

The cores were sampled at the IODP Gulf Coast Repository at the Texas A&M University, College Station, TX in 2013. We sampled four DSDP/ODP legs (Legs 66, 67, 84, 138) with their corresponding three deep-sea drilling sites on the incoming Cocos Plate (Sites 487, 495 and 845), one in the Middle American Trench (Site 499) and ten sites (Sites 488, 492, 493, 494, 497, 498, 567, 568, 569, 570) on the continental slope offshore the northern CAVA and southern Mexico for the systematic investigation of ash beds intercalated in the deep marine sediments (Fig. 1).

3.2. Methods and analytical techniques

Marine ash samples were disaggregated in an ultrasonic bath, if necessary, and subsequently wet-sieved into different grain size fractions (63–125µm, 125–250µm, >250µm and if necessary 32-63µm). The 63–125µm fraction was further used for compositional analysis of glass shards with the electron microprobe (EMP) and Laser Ablation-Inductively Coupled Plasma-Mass Spectrometry (LA-ICP-MS). All major and trace element data are given in the supplement (Supplement Tables 1-6), for standard analyses see supplement of Schindlbeck et al. (2016a) and Kutterolf et al. (2014). Sampling and analytical methods concord with the methods applied in Kutterolf et al. (2008a, 2014, 2016; 2018) and Schindlbeck et al. (2015, 2016a, 2018).

3.2.1. Electron Microprobe (EMP)

Glass shard analyses (~3500 in total) for major and minor elements were conducted on epoxy embedded samples using a JEOL JXA 8200 wavelength dispersive EMP at GEOMAR, Kiel adopting the methods from Kutterolf et al. (2011). Accuracy was monitored by standard measurements on Lipari obsidian (rhyolite, Hunt and Hill, 2001) and Smithsonian basaltic standard VGA. 60 individual glass shard measurements are bracketed by two standard measurements per standard. Standard deviations of measured elements are <0.5% for major, and <10% for minor elements (with the exception of P_2O_5 and MnO_2 in samples >65 wt% SiO_2). All analyses are normalized to 100% to eliminate the effects of variable post-depositional hydration and minor deviations in focusing the electron beam; analyses with total oxides less than 90 wt% were excluded from the data set to avoid the effects of alteration. Finally, ~3000 microprobe analyses passed the quality check which also excluded accidental shots on microcrystals. The remaining analyses for each sample were averaged (unless there was clear evidence for systematic compositional zonation) in order to characterize the elemental compositions of each individual tephra.

3.2.2. Laser Ablation-ICP-MS

Trace and selected main element concentrations of ~750 glass shards were measured by LA-ICP-MS mainly at two laboratories in Taipei, Taiwan (between 2013 and 2016) as well as at GEOMAR Helmholtz Center for Ocean Research Kiel (Germany) in April 2011.

The LA-ICP-MS analyses at GEOMAR were made using a double-focusing, magnetic sector mass spectrometer (Nu-Instruments, AttoM), which is coupled to a 193 nm Excimer laser ablation system (Coherent, GeoLasPro). Ablation was performed in a pure Helium atmosphere, additionally Argon carrier gas was mixed to the sample aerosol prior to the plasma torch. Spot analyses were done by 100 s ablation at a laser repetition rate of 3 Hz using a spot diameter of 16 µm and a fluence of 8 J/cm^2. 50 s gas background were collected prior to each ablation. Gas flows, torch position and ion-optics-focusing were optimized in order to provide a maximum in ion transparency, low oxide production rates (ThO/Th ≤ 0.3%) and fast sample wash-out. The standard NIST SRM610 glass (Wise and Watters, 2012) was used for mass calibration. Data was reduced by applying the linear regression slope method (Fietzke et al., 2008). Silicon was used for internal standardization utilizing data from EMP analyses.

The detailed machine setups, procedures, and methods of the laboratories at the National Taiwan University are described in Schindlbeck et al. (2015) and are complemented here by the description of the analytical procedures done during the measurements at the Academia Sinica (Schindlbeck et al., 2016c). The set up at the Academia Sinica in Taipei, Taiwan, comprises a laser beam (193 nm excimer laser) set to a spot size of 16 to 30 µm using 5-10 J/cm^2 energy density at 4-10 Hz repetition rate which was coupled to high-resolution ICPMS instruments. Following 45 seconds of blank acquisition, typical ablation times were around 75 seconds. Data reduction was performed using Version 4.0 of “real-time on-line” GLITTER© software (van Achterberg et al., 2001) immediately following each ablation analysis. Average silica and calcium concentrations, measured by EMP, were used as internal standards to normalize the trace element analyses. International standard glass (BCR-2G) was measured every five to eight samples to monitor accuracy and to correct for matrix effects and signal drift in the ICP-MS as well as for differences in the ablation efficiency between the sample and the reference material (Günther et al., 1999). Concentrations of NIST SRM 612, used for external calibration, were taken from Norman et al. (1996). The limit of detection (LOD) for most trace elements is generally no greater than 100 ppb. For REEs, the LOD is generally around 10 ppb. The analytical precision is better than 10% for most trace elements. Repeated measurements of the same samples in different laboratories revealed good replication of the trace elements (Schindlbeck et al., 2016a).

3.3. Correlation techniques

Geochemical fingerprinting of glass shards has been proved to be a reliable tool for tephra correlations (e.g., Lowe, 2011; Ponomareva et al., 2013; 2015; Kutterolf et al., 2008a, 2016; Schindlbeck et al., 2016a). Correlations of ash beds to terrestrial deposits as well as between different marine sites are based on major and trace element concentrations and ratios (Wulf et al., 2004; Kutterolf et al., 2008a, 2016, 2018; Schindlbeck et al., 2015, 2016a, 2018; Neugebauer et al., 2017) as well as the relative stratigraphic positions and age constraints. For each marine ash bed we carried out 15-20 EMP analyses and the majority of marine ash beds were analyzed additionally for their trace element composition by LA-ICP-MS. For reference fields of onshore deposits we used published major and trace element data (Kutterolf et al., 2008a, 2016; Stoppa, 2015; Stoppa et al., 2018). In many cases major element characteristics could not discriminate well between eruptions from single volcanoes but then the trace element compositions of volcanic glass shards provided a unique "fingerprint" for each single eruption. Next to the comparison with terrestrial deposits we also compared the investigated ash beds with data from previously studied marine drill cores (Schindlbeck et al., 2016a) and gravity cores (Kutterolf et al., 2008a) collected at the southern part of the CAVA.

3.4. Tephra ages

Age data for the marine tephra layers initially came from the shipboard age-depth models derived from magneto- and biostratigraphy from each site (Watkins et al., 1981; Aubouin et al., 1982; von Huene et al., 1985; Mayer et al., 1992). Marine tephra correlations to dated terrestrial tephra deposits (e.g., Koch and McLean, 1975; Rose et al., 1999; Kutterolf et al., 2008a; Stoppa et al., 2018) provide additional independent time markers and modified the existing age models (Fig. S1). The ages of yet undated ash layers can be estimated from their relative position between known time markers (biostratigraphic time markers, paleomagnetic time markers, correlations to independently dated terrestrial tephra deposits) by applying linear interpolation, which assumes constant sedimentation rates across such an interval. The relative position is determined from the thickness of (hemi-)pelagic sediments alone, ignoring the thickness of other intercalated ash beds (Fig. S1). We have used this method for all the marine tephra ages reported below (Tables 3, 4; Supplementary Table 1) that were not obtained by direct correlation with dated on-land deposits.

Due to compaction and drilling disturbances, the tephra ages have higher uncertainties in deeper sections of each core (e.g., up to 14% of their age; c.f. Kutterolf et al., 2013). The ages of such horizons are therefore stated as approximate values in the discussion below.

Although we can justify the assumption of constant sedimentation rates across the relatively narrow interval between two known time markers at one site, the overall sedimentation rates vary quiet significantly along the arc and with time. We observe sedimentation rates of 5-273 m/Ma on the incoming plate and 30-1540 m/Ma on the continental slope offshore Guatemala, up to 10800 m/Ma near the trench axis at the mouth of the large San José submarine canyon, and 3-284 m/Ma offshore Mexico (Fig. S1).

4 Results

4.1. Marine tephra inventory

In total, we sampled 295 ash beds and ash rich horizons and identified 223 primary ash beds characterized by homogeneous to zoned glass compositions, in contrast to ash beds with mixed, genetically unrelated glass compositions, which we interpret as reworked deposits. In addition we use the morphology and structure of the deposits to determine if they were reworked. The marine cores, especially from Legs 66 and 67, but also from Leg 84 and 138, are in parts heavily disturbed by rotary drilling (RCB) (Fig. 4); advanced piston coring (ACP) was not yet available at that time. We have sampled and analyzed tephra layers disturbed by drilling at multiple places in order to identify tephra that originally formed a single coherent layer. In these cases the stratigraphic position is determined by the uppermost occurrence of the tephra. Due to such disturbances tephra layers often cannot be correlated between even neighboring sites or holes. By combining the results from the different drill sites and holes we are confident to at least obtain a best-possible continuous record.

Although many ash beds are highly disturbed, also layers occur that are several centimeters to decimeter thick, which show normal grading and sharp contacts at the base and a diffuse transition into the background sediment at the top (Fig. 4). Analyses of the glass shards dispersed in sediment above an ash layers typically reveals that they were reworked from that layer.

The DSDP Legs 66 and 67 took place in 1979 before advanced piston coring (ACP) was available. Heavily disturbed cores and/or poor recovery thus disrupt the continuous stratigraphic record (Fig. 4). Consequently it is not surprising that tephra layers often cannot be correlated between several sites or holes although they might be in close vicinity. By combining the different drill sites we are confident to at least obtain a best-possible continuous record.

We sampled 26 ash horizons from four sites (Sites 487, 488, 492, 493) of Leg 66 offshore Mexico and identified 22 primary tephra layers. In a previous study, Cadet et al. (1982a) sampled and analyzed 15 ash beds from Leg 66. We included their major element data for three ash beds from Sites 489, 490, 491 and for four ash beds from Sites 492 and 493 that we have not sampled. Geochemical analyses identified six tephra layers as primary tephra layers at incoming plate Site 487 intercalated with hemipelagic to pelagic mud, one at the lower slope Site 488, nine at midslope Sites 490, 491 and 492 intercalated with hemipelagic mud and seven at slope Sites 489 and 493 as primary tephra layers, whereas the others represent reworked or disturbed ash horizons. The marine ash beds of Leg 66 from offshore Mexico have rhyolitic glass compositions (Fig. 5; >70 wt% SiO_2).

Eleven tephra layers were sampled from Site 845 of Leg 138, which is located ~600 km offshore of Guatemala. We identified five primary ash beds with ages obtained by shipboard age models scattering between Late Pleistocene, Early Pleistocene and Late Miocene. All five are highly evolved rhyolites (>75 wt% SiO_2; Fig. 5). Tephra layers are partly disturbed and embedded within diatom and radiolarian clay (0-136 mbsf) and nannofossil ooze (Mayer et al., 1992). Tephra thicknesses are hard to define, because the sediment is disturbed and bioturbated.

Two sites (Sites 495 and 499) were sampled from Leg 67 on the incoming plate offshore Guatemala and El Salvador. At Site 495 we took 22 samples and identified 19 primary, rhyolitic tephra layers (Fig. 5) that occur between ~12–1 Ma old sediments (Watkins et al., 1981). Site 499 is located directly within the MAT and we identified 13 primary tephra layers in Holocene to Middle Pleistocene sediments (Watkins et al., 1981). The majority of tephra layers are again highly evolved rhyolites, but we also identified one basaltic-andesitic tephra layer (~56 wt% SiO_2) (Fig. 5).

We took 224 samples from the eight slope sites from Legs 67 and 84 (Mayer et al., 1982; Aubouin and von Huene, 1985) and identified in total 164 primary ash beds embedded in Pleistocene to Early Miocene sediments. Tephra compositions are mainly rhyolitic, and occasional basaltic-andesitic to dacitic (Fig. 5). Thicknesses of tephra layers vary and contacts are often disturbed or bioturbated, which nearly precludes exact thickness determination.

The vast majority of the sampled tephra horizons are highly evolved, with SiO_2 concentrations ranging from ~70 to 78 wt.%, and total alkalis ranging from ~6 to 9.5 wt%

(Fig. 5). Only a small number of ash beds are less evolved, with SiO_2 concentrations below 60 wt% and total alkalis from 4 to 6 wt% (Fig. 5). The shard morphology for these two geochemical groups is also generally consistent, while the glass shards of the highly evolved tephra layers are transparent to light brown, with rounded and elongated bubbles, and a fibrous texture (Fig. 4). In comparison, glass shards from the less evolved group are light brownish, blocky and less vesicular (Fig. 4).

4.2. Correlation of marine tephras

In the following we will present correlations of tephra layers to specific eruptions on land, between the sites along the arc and to the source volcanic complexes. We correlated 24 tephra layers to well-known eruptions from the CAVA of the last 1.8 Ma (Figs. 6, 7) that are consecutively numbered from *C1* to *C24* (Table 3). Additional 25 tephra layers were found in multiple marine drill or gravity cores along the arc and numbered from *S1* to *S25* (Figs. 8, 9; Table 4). All other ash beds solely appear once and are consecutively numbered for each site (#xx) and are associated to the source volcanic complexes (Figs. 8, 10). Provenance analyses that are shown below identified 21 volcanic events from Mexico, 36 from Guatemala, 72 from El Salvador, as well as 14 from Nicaragua. For a subset of 14 tephra layers the identification of the exact source region was not possible, because we had no trace element information and major elements alone are not sufficiently distinctive. All established correlations are given in Table 3 and 4 and in the supplementary material. For better visualization the correlations between the sites of the last 450 ka are shown in Figure 11. Geochemical correlations to volcanic eruptions and volcanic complexes along the arcs are possible because of characteristic compositional variations from Nicaragua in the South to Mexico in the North (see Geological Background chapter). We use a large geochemical database derived from literature and own data to establish multiple provenance and correlation diagrams to correlate the marine tephra layers to known eruptions or allocate their provenance areas along the arcs (shown in Figures 6, 7, 8, 9 and 10). In the following we describe these correlations and/or source classifications with respect to their volcanic source areas from North to South.

4.2.1. Correlations to Mexico

Nineteen single ash beds from Sites 487 (# 3, 6, 9), 492 (#2, 4, 5, 7, 8), 493 (#1, 10, 11, 12), 495 (#14, 22, 29, 33), 497 (#6, 13), 498 (#5), probably originate from the Mexican volcanic arc and cover the age range from Pleistocene to Middle Miocene with a maximum age of ~15 Ma (Fig. 12). Tephra layers from the TMVB are characterized by e.g., high La/Yb (> 10) and in general low Ba/Zr (<10) (Figs. 9, 10). The along arc provenances of these tephra layers indicate volcanic sources similar to Popocatépetl and the Las Cumbres Volcanic complexes in the western part of the TMVB (Fig. 10). Additionally, two ash beds from sites offshore Mexico, associated to volcanic sources in Mexico, can be correlated to sites offshore Guatemala (*S16*, *S18*) (Fig. 8, 9; Table 4). Tephra layer *S16* (Sites 493, 492 and 568) is ~4.8 Ma and *S18* (Sites 492 and 569) ~8.2 Ma old.

4.2.2. Correlations *to Guatemala*

Atitlán- St. Maria Formation

Deposits from the Atitlán-St. Maria Formation are characterized by, e.g., high Ba/Zr (up to 25), very high Rb/Hf (up to 70) and La/Yb ratios (~8-17), but low Zr/Nb ratios (<25) (Figs. 8, 9). The tephra layer *C8* recovered at Site 569 may be correlated to the I-Fall Tephra (IFT) (Figs. 6). Koch and McLean (1975) estimated the I-Fall as >40 ka old; we determine an age of ~54 ka for tephra layer *C8*. Tephra layer *C10* is the 84 ka old Los Chocoyos Tephra (LCY), and we found the marine deposits of this large eruption in the sediment record of Sites 487, 494, 496, 497, 499, 568, 570 and 845. Correlation is based on the typical major element glass geochemistry, e.g., high SiO_2 (77.7-78.4 wt%), low CaO (~0.65 wt%) and FeO concentrations (~0.65 wt%) as well as distinctively high Ba/La ratios (>60) at low Zr/Nb ratios (<15) (Figs. 6, 7; Table 3). The LCY eruption generated a very widespread tephra layer that is not only found offshore Guatemala, but also offshore Mexico (Site 487) as well as 600 km away from the Pacific coast at Site 845. This agrees with the observation of studies in the Gulf of Mexico and elsewhere that found the marine equivalent of this eruption at large distances between Florida and Ecuador (e.g., Drexler et al, 1980; Ledbetter, 1985; Kutterolf et al., 2008a, 2016).

Tephra layer *C13* correlates with the 158 ka W-Fall Tephra (WFT) (Sites 496, 497, 567 and 568) characterized by high K_2O (typically around ~5 wt%) and silica contents (77–78 wt%) as well as the highest La/Yb ratio (14–20) in Northern CAVA tephras (Figs. 6, 7; Table 3). Tephra layer *C15 (*Sites 487, 488) is the Atitlán Older Tephra (AOT), which is probably ~306 ka old (Figs. 6, 7; Table 3) and shows the same compositional signature as Los Chocoyos, but can be distinguished by its stratigraphic position. This tephra has been found in the lake sediments of Lake Petén Itza in Northeast Guatemala as well as in some Pacific gravity cores offshore El Salvador (Kutterolf et al., 2016, 2008a).

The two tephra layers *S6* (0.51 Ma; Site 494) and *S7* (~0.57–0.54 Ma; Site 494) are correlated with marine ash beds from gravity cores taken during Meteor cruise M66 (core M66-230 offshore El Salvador) and contain the high Ba/Zr (~13) and Rb/Hf (55) ratios that are characteristic for eruption products from Atitlán Caldera (Figs. 8, 9; Table 4). Tephra layer *S19*, with similar trace element compositions, is correlated between Sites 567 and 568 and associated with an eruption from Atitlán at ~13.9 Ma. Tephra layer *S21* (~14.4 Ma; Sites 568 and 569) has a bimodal composition at Site 569 indicating a mix of Guatemalan and El Salvadorian ash (Figs. 8, 9; Table 4; Supplement Table 1).

Two single ash beds at Sites 497 (#2) and 569 (#3) can be compositionally associated with eruptions from Atilán Caldera at 414 and 421 ka. Three single ash beds at Site 570 (#19; 2.76

Ma) and Site 845 (#1; ~2.45 Ma) are also associated with Atitlán Caldera. Four single ash beds in the Miocene sediments of Sites 495 (#42, 11.9 Ma), 568 (#40, 15.4 Ma; #43; 15.5 Ma) and 569 (#49; 22.4 Ma) are geochemically similar to the W-Fall Tephra and therefore probably associated with an old eruption from Atitlán (Figs. 8, 10; Supplement Table 1).

Amatitlán-Antigua Formation

The Amatilán-Antigua Formation is characterized by e.g., Zr/Nb ratios > 15, Ba/La ratios between 40-70 and high Rb/Hf ratios <40 (Figs. 8, 9). Tephra layer *C5* is the 50 ka E-Fall Tephra (EFT) that was recovered at Sites 496, 498, and 568. This correlations is based on the typical glass composition with high SiO_2 concentrations (~76–77 wt%) and CaO contents of ~0.9 wt%, but especially on the specific trace element compositions (e.g., Ba/La ~45–55; Zr/Nb ~15–20) (Fig. 6, 7; Table 3; Supplement Table 1). The marine deposits of the 191 ka L-Fall Tephra were found offshore Guatemala, but also offshore Mexico at Sites 487, 570, 845 (*C14*; Figs. 6, 7). Both E-Fall and L-Fall Tephras have high potassium contents (>4.4 K_2O wt%), contain biotite and are also deposited in the Gulf of Mexico (Rabek et al., 1985; Kutterolf et al., 2016), which illustrates their wide distribution and large eruption magnitude. Although EFT and LFT have very similar glass compositions it is possible to distinguish them by their relative stratigraphic position relative to LCY (84 ka).

Two tephra layers (*S22, S25*) can be correlated between Sites 569 and 494 offshore Guatemala (Figs. 8, 9; Table 4; Supplement Table 1), are Miocene in age (~15.8 and ~21.5 Ma), and are geochemically similar to Amatitlán (high SiO_2 ~77.5–78 wt%; high K_2O ~4.5–5 wt%; Rb/Hf ~27-49).

Ten single ash beds from Sites 568 (#44; ~15.6 Ma), 569 (#8, 13, 47 and 48; ~1.19, 1.33, 21.5 and 21.7 Ma) and 570 (#21, 22, 29 and 30; 3.49, 4.19 and 6.63 Ma) and 494 (#47; 22.1 Ma) are also compositionally correlated to the Amatitlán-Antigua Formation (Figs. 8, 10).

Ayarza Formation

Deposits of the Ayarza Formation have typically e.g., low Ba/Nb (<100) and Zr/Nb ratios (<10) and moderate high Rb/Hf ratios (>30). Tephra layer *C4* (Sites 496, 499, 570) correlates with the chemical fingerprint of the 39 ka Mixta Fall from the Ayarza Caldera. The correlation is based on the distinctive major element composition with very low CaO (~0.4 wt%) and MgO (<0.1 wt%) contents at high K_2O (~4 wt%) and SiO_2 (~77 wt%) contents. Characteristic are the low Zr/Nb (<7) and Ba/Rb ratios (<7) at Ba/La ratios between ~40 and 60 (Figs. 6, 7; Table 3; Supplement Table 1).

Furthermore we geochemically correlated an ash bed from Site 569 with an ash layer from the southern CAVA (tephra layer “s21” from Schindlbeck et al. (2016a)), which is probably from an ~1 Ma eruption from Ayarza or Atitlán (tephra layer *S9*; Fig. 6, 7). Another correlation between Sites 493 and 568 is tephra layer *S20* (14.5–14.3 Ma) that is geochemically similar to Ayarza, but also has similarities with deposits known from Ataco Caldera (Figs. 8, 9; Table 4; Supplement Table 1).

4.2.3. Correlations to El Salvador

Coatepeque-Ataco Formation

The Coatepeque-Ataco Formation covers a large geochemical range, but many eruptions have low Ba/La ratios (<60), and low Rb/Hf ratios (<40), but high Ce/Pb ratios (>2.5) and high potassium contents (K_2O>3.5 wt%). Marine layer *C6* (Site 497, 499, 568) is compositionally equivalent to the 53 ka Congo Tephra (CGT) from the Coatepeque Caldera, El Salvador. Deposits of the CGT are characterized by SiO_2 of ~74 wt%, but high K_2O (>4.2 wt%) and CaO (>1.1 wt%) contents (Fig. 6). Major element compositions overlap with compositions of the Conacaste Tephra, but trace elements (e.g., especially lower Zr/Nb <30) help to distinguish between these also temporally closely related eruptions. Additionally, we correlated marine tephra layer *C9* with the 72 ka Arce Tephras (L/UACT) and *C12* (Site 568) with the Old Arce Tephra (OACT) (Figs. 6, 7). The correlation is supported by the high K_20 contents (4.8–5.5 wt%) as well as the exceptional low Ba/La (<20) and Ba/Zr (<7) ratios. Furthermore, tephra layer *C16* at Site 497 has the same major element composition as the ~400 ka Ataco Tephra 3 (AC3) (Fig. 6; Table 3; Supplement Table 1) with relatively low SiO_2 contents (~71 wt%) and ~3 wt% K_2O.

The older marine tephra layers *S17* (Sites 495 and 569; ~6.3 Ma), *S20* (Sites 493 and 568; 14.5–14.3 Ma) and *S23* (16.6–15.9 Ma) can be correlated between Sites 494, 496 and 569 (Figs. 8, 9; Table 4; Supplement Table 1) and also show the compositional characteristics of volcanic products from the Coatepeque/Ataco complex.

Furthermore, seventeen single ash beds show the characteristic geochemical fingerprint known from the Ataco and Coatepeque Calderas (Supplement Table 1). Two ash beds from Site 569 (#7 and #31; ~1 Ma and 8.1 Ma) and one from Site 497 (#32; 2.8 Ma) have the geochemical signature of the Ataco Caldera (Figs. 8, 10). Additionally, another four older single ash beds between 15.6 and 14.2 Ma are geochemically similar to the Ataco Caldera (#36, 37, 38 and 44 from Site 568). Ten single ash beds in the sediments offshore Guatemala can be correlated to the Coatepeque-Ataco Formation (Figs. 8, 10). Except tephra layer #9 (Site 499; 1.55 Ma), all of the other layers have been deposited in the Miocene [#34 (Site 497), #40 (Site 495), #41 (Site 498), #43 and 44 (Site 496), #39, 45 and 46 (Site 569) and #41 (Site 568)] between 21.1 and 6.3 Ma.

Ilopango and Apopa-Cojutepeque Formation

The Ilopango Formation is known for high Ba/La (>60), Ba/Zr (up to 20) and Zr/Nb ratios (>25) at moderate to high potassium and calcium contents (3 to 5 wt% K_2O, >~1wt% CaO) for silica contents >76 wt% SiO_2 (Figs. 6,8,9). We correlate the Terra Blanca Joven (TBJ) eruption (1.5 ka) to a tephra in the uppermost centimeters of Site 499 (*C1*), as well as the 36 ka Terra Blanca 4 (TB4) eruption to tephra layer *C3* at Sites 496, 499, 568 and 570 (Figs. 6, 7; Table 3). The correlations are based on the characteristic glass shard major and trace element compositions as well as the relative stratigraphic position in the cores. The deposits of TBJ and TB4 have relatively low K_2O (<3 wt%) at high SiO_2 (>76 wt%) (Fig. 6). Even more distinctive is the trace element composition with typically high Ba/Th ratios (>300) and high Ba/La ratios (>85) (Fig. 7; Table 3; Supplement Table 1). Marine tephra layer *C11* that was recovered at Site 494 corresponds to the 80 ka Old Ilopango Tephra (OPI), which is supported by the stratigraphic position and the same major element signature as TBJ and TB4 eruption products (Fig. 6; Table 3). Not so much is known about the older Pleistocene eruptions from Ilopango Caldera (Kwasnitschka, 2009), but we found the Feliz Tephra (*C19*; 0.66 Ma at Site 569), the Salvamex Tephra (*C21*; 1.03 Ma at Site 495) and the La Curva Tephra (*C22*; 1.15 Ma at Site 569) as marine equivalents in the sediments offshore Guatemala (Table 4; Supplementary Table 7). These are the first age constraints for the older Ilopango succession exposed along the Pan American Highway North of the caldera (Kwasnitschka, 2009), which fills the gap between the Terra Blanca succession and ~2 Ma old ignimbrites South of the caldera.

Moreover, site to site correlated tephra layers *S8* (Sites 568 and 570; 0.6 Ma) *S10* (Sites 497 and 568; ~1.3 Ma), *S11* (Sites 495, 496, 497 and 568; ~1.6 Ma), *S12* (Sites 568 and 570; 2.2 Ma), *S13* (Sites 495 and 570; 2.32–2 Ma), *S15* (Site 494 and 496; 3–2.9 Ma) and *S24* (Sites 494 and 569; 17.4-17 Ma) are probably from eruptions from the Ilopango area, assuming that magmatic compositions remained similar throughout that time span. However, tephra layer *S12* shows also some geochemical similarities with Atitlán (Figs. 8,9; e.g., high Ba/Zr; Table 4; Supplement Table 1).

Additionally, there are at least 28 single ash beds (Figs. 8, 10) that can be compositionally attributed to older formations at Ilopango reaching back until ~16.5 Ma [Sites 499 (#10; 1.58

Ma), 495 (#19; 1.92 Ma), 496 and 497 (#3, 4, 28, 31, 35, 36, 37, 38, 45, 46), 845 (#2); 499 (#11), 568 (#23, 24, 25, 26, 27, 42), 569 (#2, 3, 4, 10, 11, 14, 32) and 570 (#5,18)].

St. Vicente-Apastepeque Formation

Eruptions from the St. Vicente-Apastepeque Formation are geochemically similar to the Ilopango Fomation, but have in general lower Rb/Hf and La/Yb ratios (<15 and ~5 respectively; Figs. 8, 9). The Upper and Lower Apastepeque Pumice (UPT and LPT) are the oldest known eruptions from the St.Vicente-Apastepeque Formation on land but no age constraints have been found so far (Fig. 3). We probably found the marine deposits of both eruptions in the sediments of Site 499 applying compositional fingerprinting (tephra layers *C20* and *C23*; Figs. 6). The Apastepeque Pumice on land has silica contents of ~76 wt% with lower K_2O contents (2.8–3.1 wt%), but higher FeO (1.5–1.6 wt%) and CaO (1.4–1.6 wt%) contents (Fig. 6). The calculated ages for these eruptions are ~0.88 and ~1 Ma. Additionally, one single ash bed at Site 495 (#15; 1.81 Ma) can probably be associated with an even older eruption from this volcanic complex.

Berlin-Chinameca Formation

The Berlin-Chinameca Formation is the southernmost tephra formation in El Salvador and geochemically characterized by e.g. low Pb/Nd (<0.5) and low Rb/Hf (<12), but high U/Th (0.4-0.8), and Zr/Nb (>30) ratios (Figs. 8, 9). Tephra layer *C7* correlates to the Berlin-Chinameca complex and specifically to the 56 ka Old Pacayal Tephra (OPT), which Kutterolf et al. (2008a, 2016) also found as a marine tephra in gravity cores of RV Meteor cruise M66 and as an ash layer in sediments of Lake Petén Itza. Next to its compositional similarity (~57 wt% SiO_2; very high Ba/Th ~460 and Ba/Rb >30) *C7* also fits into the relative stratigraphic order known from previously studied onshore, lacustrine and marine sediments in this region (Fig. 7; Supplement Table 1).

There are additionally four single ash beds identified at Site 494 and one at Site 495 that are geochemically similar to the Berlin-Chinameca Formation, but also show some similarities with the St. Vicente-Apastepeque Formation (Figs. 8, 10). These tephras were deposited between 1.5 and 2.2 Ma (#8, 16, 17 and 25; Site 494 and #20; Site 495).

4.2.4. Correlations to Nicaragua

Typical for the Nicaraguan part of the CAVA are geochemical compositions with very high Ba/La (up to 140) and Ba/Th (>400) ratios, but very low Rb/Hf ratios (<10) (Figs. 8, 9). Tephra layer *C2* is correlated with the 24.5 ka Lower Apoyo Tephra (LAT), product of a Plinian eruption from Apoyo caldera in Nicaragua, which has very specific potassium, iron, magnesium and calcium contents at high silica values compared to other CAVA tephras in this age range. Kutterolf et al. (2008a) used these compositional characteristics to show that ash from the LAT eruption has been dispersed westwards across the Pacific, which fits our detection of layer *C2* at Site 569.

The Malpaisillo Caldera in Nicaragua has produced several large eruptions. In the cores offshore Guatemala we correlate the 420 ka Tolapa Tephra (TolT; *C17*; Sites 494 and 570) and the 450 ka La Sabanetta Tephra (LSabT; *C18*; Site 497) to ash layers in the sediments offshore Guatemala. The correlations are based on major and trace element glass compositions (Figs. 6a,b,d, 7b,f), whereby the very high Ba/Th (>400) and Ba/La (>110) ratios of the Malpaisillo rocks are particularly helpful. Additionally tephra layer *C24* can be assigned to the Lower Boulevard Bio Pumice (LBBP; Site 494; 1.8 Ma) originated from an unknown source in Central Nicaragua, with typically high CaO (~2-3 wt%) at low K_2O (<2.7 wt%) contents (Figs. 6a,b,c, 7b,f; Table 3; Supplement Table 1).

Furthermore, we correlated several, mostly mafic, tephras from Nicaragua between marine sites that suggest an origin from the Masaya/Las Sierras volcanic complex in central Western

Nicaragua (Supplement Table 1). Tephra layer *S1* (0.1 Ma) is a correlation between Site 496 and a marine gravity core M66-223_69-76 cm (Kutterolf et al., 2008a). Tephra layer *S2* (0.16 Ma) can be correlated with tephra layer "s3" from Schindlbeck et al. (2016a), which is a widespread tephra that can be found in multiple ODP and IODP sites in the Pacific (Sites 1039, 1254, 1255, U1381 and U1414). Tephra layers *S3, S4* (0.18 and 0.21 Ma; Site 496) and *S5* (~0.4 Ma; Sites 496, 497 and 569), can be correlated to marine tephra layers from Sites 1242 and U1381 offshore Costa Rica (tephra layer "s10" from Schindlbeck et al., 2016a). The 2.26 Ma felsic tephra layer *S14* can be found in the sediments of Site 495 and Site 1039 offshore Costa Rica (Figs. 8, 9; Table 4); this tephra layer might originate from the Tertiary Coyol arc (Ehrenborg, 1996) in the highlands of Nicaragua, 100 km east of the modern Nicaraguan arc (Schindlbeck et al., 2016a).

Additionally, five single felsic ash beds from Sites 497 (#12 and 39; 1.6 and 5.7 Ma), 569 (#15 and 16; 1.39 and 1.52 Ma) and 570 (#20; 3.39 Ma) probably originated from Nicaraguan eruptions as well, as respective provenance diagrams indicate (Figs. 8, 10).

5 Implications for North Central American volcanism

To understand the temporal evolution of the explosive volcanism in Central America as well as the evolution and distribution of specific eruptions it is necessary to study a long and most complete record. The major problem on land is the lack of outcrops of old deposits due to extensive erosion and successive coverage by younger deposits. Even more complicated are relative age estimates in case of missing stratigraphic relationships. The marine tephra record provides the opportunity 1) to extend and complete the record of explosive eruptions for the individual volcanic centers and regions along the arcs, and 2) to build a temporal framework using the age estimations derived from marine sedimentation rates.

5.1. Age implications for terrestrial eruptions

We obtained eight new ages for already known, but so far undated eruptions from Nicaragua, El Salvador and Guatemala. Our dating of the I- Fall Tephra (IFT) to ~ 54 ka by correlation to marine tephra layer *C8* at Site 569 (Figs. 6, 7, S1), also defines the time when the period of huge explosive eruptions from Atitlán caldera ended. This caldera thus produced its nine large-volume widespread tephras from 158 to 54 ka.

.The recent eruptive history at Ilopango caldera is recorded in the well-known Terra Blanca Tephras (<36 ka; Kutterolf et al., 2008a). The underlying thick and complex tephra succession has been stratigraphically logged by Kwasnitschka (2009) but the only age constraint is the ignimbrite (1.77±0.22 Ma – 1.81±0.22 Ma; Lexa et al., 2011) below an unconformity at the base of the sequence. We found three tephras of that succession in the marine cores at 0.66, 1.03 and 1.15 Ma (layers *C19, C21, C22*). The respective tephra beds (Feliz Tephra, Salvamex Tephra, La Curva Tephra) belong to the Cojutepeque unit of Kwasnitschka (2009), which is overlain by the Soyapango (seven tephras) and Apopa (five tephras) units (Fig. 3). The new ages imply that the Soyapango and Apopa tephras were emplaced between <660 to >36 ka, and that tephras below the Cojutepeque unit (>1.15 Ma) are associated with the older ignimbrite succession.

The previously undated Upper and Lower Apastepeque Pumice tephras (UPT and LPT; >2 m thick each) from Apastapeque Caldera were erupted at of ~0.88 and ~1 Ma as inferred from correlation to marine tephra layers *C20* and *C23*. They are thus much older than we had previously assumed (cf. Fig. 3) and imply a considerable time gap between Apastepeque caldera and St. Vicente volcanic activity.

For Nicaragua, the ~450 ka age of La Sabanetta Tephra, correlated to layer *C18* (Site 497), fits the results from the recent study of the Malpaisillo Formation by Stoppa et al. (2018), who radiometrically dated the directly overlying Tolapa tephra (420±40 ka) and the 570±70 ka old La Paz Centro Tephra at the base of the Malpaisillo Formation (Stoppa et al., 2018).

Finally, the Boulevard Bio Pumice obtains the ~1.8 Ma age of marine tephra layer *C24* (Site 494). This age suggests its origin from the late stages of the Tertiary Coyol arc in Central Nicaragua.

5.2 Temporal evolution of explosive volcanism along the arcs

The investigated marine tephra record offers the opportunity to study the history of the explosive eruptions from the different regions and volcanic complexes along the arc back in time. In Figure 12 the temporal distribution of eruptions is shown along the arc, each tephra is associated with the respective volcanic complex/region that we have assigned by geochemical correlations.

Newhall (1987) postulated three caldera stages (11 Ma, 8 Ma and 84 ka) for the Atitlán volcanic complex. The marine tephra layers between ~14–12 Ma and >21 Ma are probably associated with eruptions from the first Atitlán stage or an even older, previously not recognized stage. However, we do not see any evidence for explosive eruptions from the second stage (8 Ma) in the marine cores. Stage three comprises nine major eruptions from 158 to 54 ka (WFT to IFT) of which the extremely voluminous Los Chocoyos eruption (84 ka) was a main caldera forming event. However, new observations on dispersal characteristics yield large volumes also for other events; for example, the ~0.16 Ma WFT tephra has an updated erupted volume of ~90 km^3 DRE ((Kutterolf et al., 2008a, 2016). Hence, the third Atitlán Caldera may not have formed by the LCY eruption alone (Newhall, 1987; Rose et al., 1987), but may represent a nested caldera with subsidence phases at least after each of the large WFT and LCY eruptions. Moreover, marine ash layers at around 300 ka (*C15* = AOT) and around 500-600 ka (*S6*, *S7*) document large explosive eruptions at Atitlán preceding the main stage three.

The eruption record from the Amatitlán volcanic complex reaches continuously back until ~7 Ma (Fig. 12), which is much longer than previously known from land. Koch and McLean (1975) described the R-tephra as representing at least five old (>0.5 Ma) eruptions from Amatitlán Caldera. However, we have found evidence for activity in the Amatitlán area during the Middle (~16–14 Ma) and Early Miocene (~23–21 Ma), at similar times as for Atitlán Caldera as well as for the Coatepeque and Ilopango calderas in El Salvador (Fig. 12).

The Coatepeque/Ataco volcanic complex is the only one that has a more or less continuous record of tephras in the marine cores reaching back into the Early Miocene. However, this might represent a sampling bias since the region around the Coatepeque Caldera is closest to many drill sites (~160 km; Leg 67, 84), which might favor the preservation of smaller explosive eruptions in the marine sediments.

There are abundant marine tephras that originate from the Ilopango region (~200 km to Leg 67 and 84), especially during the last ~6 Myr, but volcanism was also active during the Late (10–8 Ma) and Middle (16–14 Ma) Miocene (Fig. 12). Explosive eruptions associated with the Berlin-Chinameca complex, however, are limited to the last ~ 3 Myr (Fig. 12).

Several correlations to the mafic Las Sierras Formation in Western Nicaragua assist the longevity of the associated magmatic system over at least the last 400 kyr as it has been proposed by Schindlbeck et al. (2016a, b).

The eruption records derived from the marine deposits indicate a long history of explosive volcanism for the major volcanic complexes reaching back into the Early Miocene (Fig. 12).

However, for Nicaragua (and partly Honduras), where slab roll-back caused a trench-ward shift in the position of the volcanic front, the older Tertiary tephras must derive from volcanoes at the now extinct Coyol arc (Ehrenborg, 1996). Yet the geochemical characteristics of these tephras are very similar to those of tephras from the Quaternary volcanic front (Jordan et al., 2007b; Nyström et al., 1988). This suggests that, despite the roll-back, subduction conditions controlling magmatic compositions did not change much over the last 25 Myr.

5.3 Global episodes of enhanced volcanic activity

At the bottom of Figure 12 we show how the frequency of large eruptions at the major volcanic centers varies over time. The interesting observation is that many centers share time intervals of increased activity. This suggests that there may be some process controlling eruption frequency that operates at a scale at least covering the entire subduction zone length. We thus also show a total frequency distribution over time for the entire subduction zone from Nicaragua to Mexico.

This distribution indicates five pulses of enhanced explosive volcanic activity (Fig. 12): 1) a pulse during the Quaternary, 2) a Pliocene pulse between 6 and 3 Ma, 3) a Late Miocene pulse between 10 and 7 Ma, 4) a Middle Miocene pulse between 17–11 Ma, and 5) an Early Miocene pulse (~>21 Ma). Several authors postulated episodic volcanic activity in Central America (e.g., Kennett et al., 1977; Reynolds, 1980). Reynolds (1980) studied effusive and explosive eruption products, and proposed three Neogene episodes of volcanism for Guatemala, El Salvador and Honduras. He defined three major formations that extruded during the Middle and Late Miocene (Chalatenango Formation), during the Late Miocene to Pliocene (Bálsamo Formation) and during the Pliocene to Pleistocene (Cuscatlán Formation). Although the study of Reynolds (1980) lacked good age control of the studied deposits, the overall observation of episodic volcanism is probably correct and the pulses agree well with our findings.

The tephra record from Mexico covers eruptions from the Middle Miocene to the Holocene with gaps between ~13–10 Ma (only one eruption) and between 8–5 Ma. This might either feature a real decrease in explosive volcanism or a sampling and preservation problem. Ferrari et al. (1999) postulated that volcanism in Mexico occurs in pulses with peaks between 31–28 Ma, 23 Ma, 10.5–9 Ma and since 5 Ma. Indeed, we also see an increase in eruption frequency between 10 and 8 Ma and since 5 Ma (Fig. 12).

Several studies postulated that volcanic activity occurs in episodes (e.g., Kennet and Thunell, 1975). Comparing our data with published pulses in volcanic activity at different regions around the ROF and with global climate and tectonic events indicates some temporal coincidences (Fig. 13).

Kennett et al. (1977) were the first to describe two major pulses at 2–0 and 16–14 Ma, as well as two less pronounced periods of enhanced effusive and explosive volcanism between 6–3 and 11–8 Ma for the Southwest Pacific, Central America and the Cascades (Fig. 13). The same pulses were also recognized in a tephra compilation from several DSDP sites and especially in Legs 66 and 67 (Kennett and Thunell, 1975; Kennett et al., 1977; Cadet et al., 1982a, b). Marine tephra records from Japan indicate similar periods of increased explosive volcanic activity between 2–0, 6–4, ~8 and possibly 15–13 Ma (Mahony et al., 2016) (Fig. 13). In the Caribbean, Carey and Sigurdsson (2000) and Sigurdsson et al. (2000) studied the temporal distribution of ash beds at several ODP sites. They found periods of enhanced ash accumulation in the marine sediments of ODP Leg 165 during the Late Miocene (~11–7 Ma) and the Early to Middle Miocene (>12 Ma) as well as during the Oligocene and Eocene (Fig. 13). Sigurdsson et al. (2000) already noted that their Late Miocene and Early–Middle

Miocene peaks agree with results of Kennett and Thunell (1977) and Cadet et al. (1982a, b) although with a small temporal offset. The pronounced Quaternary and the Pliocene peaks, however, were not detected in the Caribbean tephra records (Fig. 13). Our Pacific Central American record does, however, support all periods of enhanced eruption activity at <2 Ma, 3–6 Ma, 7–10 Ma, 11–17 Ma and thus agrees with other regions around the ROF, allowing for some minor deviations in individual lengths of episodes.

Possible causes for these pulses of enhanced volcanic activity are thought to be related to changes in large-scale plate tectonics (e.g., Mahony et al., 2016), or to climate influencing the lithospheric regime by suppressing or favoring magma ascent (e.g., glacial loading and unloading; e.g., Rampino et al., 1979; McGuire et al., 1997) or by affecting erosion and sedimentation rates. For example, Sigurdsson (1990) attributed variations in marine sedimentation rates to changes in atmospheric circulation due to climate changes. Von Huene and Scholl (1992) suggested that a larger amount of subducted sediments during the Quaternary led to an increase in arc volcanism over the last 2 Myr.

While our data cannot constrain any physical processes, we do observe some temporal coincidences between tectonic, climatic and volcanic events globally.

(1) The break-up of the Farallon into the Cocos and Nazca plates at about 23 Ma and subsequent rearrangements in the subduction zone caused large-scale topographic uplift and extension in northern Central America (Mann et al., 2007), which may have enhanced volcanism. Additionally, this is also the time of super-fast spreading on the East Pacific Rise, which lead to an increase in the convergence rate at the Middle American Trench. The Mid-Miocene pulse in volcanism also coincides with the peak in the Columbia River flood basalt volcanism associated with widespread extensional tectonics in western North America (Kohn and Fremd, 2008), which indicates tectonic rearrangements along the Pacific-American

boundary. The rapid rise of orogenic plateaus during this period (e.g., Tibetan Plateau, Himalaya), probably associated with changes in global plate tectonics, induced changes in global climate (Kohn and Fremd, 2008). For instance, the Mid-Miocene climatic transition from optimum to disrupted conditions influenced bioproductivity and therefore character and amount of sedimentation on the down going plates along the ROF that may have influenced the magma generation at the arc systems ROF-wide. The Mid-Miocene transition also marks the beginning of the interplay of cold and warm periods due to orbital forcing (Holbourn et al., 2005), which may have influenced the volcanism in the Mid-Miocene.

(2) During the period of high volcanic activity between 10 and 7 Ma northern Central America was bracketed between tectonic events in the north and in the south. In Mexico, the 11.5-6 Ma period of eastward migrating intense volcanism followed the eastward propagation of a slab tear that ultimately led to slab detachment and reduction of convergence rates (Ferrari, 2004). In Nicaragua, slab rollback from 10–4 Ma caused associated extension (Mann et al., 2007). In the global perspective, 10 to 7 Ma intense volcanic period coincides with the Late Miocene global cooling (Herbert et al., 2016) and the onset of the Miocene reglaciation of the Antarctic ice sheet with global climatic consequences such as the intensification of the Asian monsoons (Ao et al., 2016). The episodic pattern of enhanced ice-rafted debris deposition during times of deglaciation provides evidence that the Late Miocene east Antarctic ice sheets underwent dynamic large size variations at orbital time scales (Grützner et al., 2003), implying periodic changes in isostatic loading of the ocean plates and the continents, but also the respective sedimentation (dust) on the ocean crust.

(3) The episode between 6 to 3 Ma coincides with the proposed closure of the Panama isthmus associated with changes in plate direction and velocities possibly affecting magma generation at the Central American arc. This coincidence may be questionable since the exact

timing of the closure is still under debate and the Caribbean volcanic record, close by, does not show this pulse.

In summary it seems that there is an interplay of tectonic and climatic forcing on the volcanic systems at the ROF or even globally that controls the activity on long timescales, but further studies are needed to understand the physical mechanisms.

5 Conclusions

We provide a stratigraphically classified tephra database of glass compositions of large-magnitude Quaternary to Neogene explosive eruptions at Central America, together with correlations of marine tephra layers to their terrestrial counterparts and source regions along the volcanic arcs. Additionally, we used the marine sedimentation rates in combination with tephra correlations to independently date terrestrial deposits to build a chronotephrostratigraphy and obtained new ages for several eruptions already known on land. These data provide new insights into the overall lifetime and the number of major eruptions of the major volcanic centers in Guatemala and El Salvador. Volcanism in North Central America probably occurred in episodes since the Miocene with five pulses of enhanced activity during the Quaternary, the Pliocene (6–3 Ma), the Late Miocene (10–7 Ma), the Middle Miocene (17–11 Ma), and the Early Miocene (~>21 Ma).

Acknowledgements, Samples, and Data

The Integrated Ocean Discovery Program provided shipboard data and samples. We appreciate the help of IODP staff during sampling in College Station, TX. The German Research Foundation funded this project (grant KU-2685/2-1&2). We kindly thank K. Strehlow, I. Rohr, T. Wollenschläger and K. Fockenberg for sample preparation and M. Thöner, J. Fietzke, D. Rau, F. Lin, Y. Chien and C. Hung for lab assistance. We appreciate the comments from two anonymous reviewers, which helped to improve the manuscript. The authors declare no real or perceived financial conflicts of interests. All data is available in the supporting information.

References

Abers, G. A., Plank, T., & Hacker, B. R. (2003). The wet Nicaraguan slab. *Geophysical Research Letters, 30*(2). doi: 10. 1029/2002GLO 15 649.

Ao, H., Roberts, A. P., Dekkers, M. J., Liu, X., Rohling, E. J., Shi, Z., . . . Zhao, X. (2016). Late Miocene–Pliocene Asian monsoon intensification linked to Antarctic ice-sheet growth. *Earth and Planetary Science Letters, 444*, 75-87.

Arana-Salinas, L., Siebe, C., & Macías, J. L. (2010). Dynamics of the ca. 4965 yr 14C BP "Ochre Pumice" Plinian eruption of Popocatépetl volcano, México. *Journal of Volcanology and Geothermal Research, 192*(3-4), 212-231.

Arce, J., Cervantes, K., Macías, J., & Mora, J. (2005). The 12.1 ka Middle Toluca Pumice: A dacitic Plinian–subplinian eruption of Nevado de Toluca in central Mexico. *Journal of Volcanology and Geothermal Research, 147*(1), 125-143.

Arce, J., Gardner, J., & Macías, J. (2013). Pre-eruptive conditions of dacitic magma erupted during the 21.7 ka Plinian event at Nevado de Toluca volcano, Central Mexico. *Journal of Volcanology and Geothermal Research, 249*, 49-65.

Arce, J., Macías, J., Gardner, J., & Rangel, E. (2012). Reconstruction of the Sibinal Pumice, an andesitic Plinian eruption at Tacaná Volcanic Complex, Mexico–Guatemala. *Journal of Volcanology and Geothermal Research, 217*, 39-55.

Arce, J. L., Macias, J. L., & Vázquez-Selem, L. (2003). The 10.5 ka Plinian eruption of Nevado de Toluca volcano, Mexico: Stratigraphy and hazard implications. *The Geological Society of America Bulletin, 115*(2), 230-248.

Aubouin, J., & von Huene, R. (1985). Summary; Leg 84, Middle America Trench transect off Guatemala and Costa Rica. *Initial reports of the Deep Sea Drilling Project covering Leg 84 of the cruises of the Drilling Vessel Glomar Challenger; Balboa, Panama, to Manzanillo, Mexico, January-February 1982, 84*, 939-957.

Barckhausen, U., Ranero, C. R., von Huene, R., Cande, S., & Roeser, H. (2001). Revised tectonic boundaries in the Cocos Plate off Costa Rica: Implications for the segmentation of the convergent margin and for plate tectonic models. *Journal of Geophysical Research, 106*(19), 207-220.

Bloomfield, K., & Valastro Jr, S. (1977). Late Quaternary tephrochronology of Nevado de Toluca volcano, central Mexico. *Overseas Geology and Mineral Resources (UK). no. 46.*

Bloomfield, K., & Valastro, S. (1974). Late Pleistocene eruptive history of Nevado de Toluca volcano, central Mexico. *Geological Society of America Bulletin, 85*(6), 901-906.

Boudal, C., & Robin, C. (1989). Volcán Popocatépetl: recent eruptive history, and potential hazards and risks in future eruptions *Volcanic hazards* (pp. 110-128): Springer, Berlin, Heidelberg.

Bowles, F. A., Jack, R. N., & Carmichael, I. S. E. (1973). Investigation of deep-sea volcanic ash layers from equatorial Pacific cores. *The Geological Society of America Bulletin, 84*, 2371-2388.

Cadet, J.-P., Pouclet, A., Thisse, Y., Bardintzeff, J. M., & Azéma, J. (1982a). Middle America Neogene explosive volcanism and ash layers: evidence from the Middle America Trench transect, Deep Sea Drilling Project 67. In J. Aubouin, R. von Huene, & e. al. (Eds.), *Initial Reports DSDP* (Vol. 67, pp. 475-491). Washington: U.S. Govt. Printing Office.

Cadet, J.-P., Thisse, Y., Pouclet, A., Bardintzeff, J.-M., & Stephan, J.-F. (1982). Tephra from Deep Sea Drilling Project Leg 66; Middle America Trench transect (southern Mexico). *Leg 66 of the cruises of the drilling vessel Glomar Challenger; Mazatlan, Mexico to Manzanillo, Mexico; March-May, 1979, 66*, 687-698.

Cameron, B. I., Walker, J. A., Carr, M. J., Patino, L. C., Matias, O., & Feigenson, M. D. (2002). Flux versus decompression melting at stratovolcanoes in southeastern Guatemala. *Journal of Volcanology and Geothermal Research, 119*, 21-50.

Carey, S., & Sigurdsson, H. (2000). Grain size of Miocene volcanic ash layers from Sites 998, 999, and 1000: Implications for source areas and dispersal. In R. M. Leckie, H. Sigurdsson, G. D. Acton, & G. Draper (Eds.), *Proceedings ODP, Scientific Results 165* (pp. 101-110).

Carey, S. N. (2000). Volcaniclastic sedimentation around island arcs. In:. In H. e. a. Sigurdsson (Ed.), *Encyclopedia of volcanoes* (Vol. Academic Press, pp. 627-642).

Carr, M., Feigenson, M. D., Patino, L. C., & Walker, J. A. (2003). Volcanism and Geochemistry in Central America: Progress and Problems, Inside the Subduction Factory. *AGU special publication, Geophysical Monograph 138*, 153-174.

Carr, M. J. (1984). Symetrical and segmented variation of physical and geochemical characteristics of the Central American Volcanic Front. *Journal of Volcanology and Geothermal Research, 20*, 231-252.

Carr, M. J., Feigensohn, M. D., & Benett, E. A. (1990). Incompatible element and isotopic evidence for tectonic control of source mixing and melt extraction along the central American arc. *Contributions to Mineralogy and Petrology, 105*, 369-380.

Carr, M. J., Patino, L. C., & Feigenson, M. D. (2007). Petrology and geochemistry of lavas. In J. Buntschuh & G. E. Alvarado (Eds.), *Central America – Geology, resources and hazards*. Rotterdam, Netherlands: Balkema, 565-591.

Carrasco-Nunez, G., & Rose, W. I. (1995). Eruption of a major Holocene pyroclastic flow at Citlaltepetl volcano (Pico de Orizaba), Mexico, 8.5-9.0 ka. *Journal of Volcanology and Geothermal Research*, *69*, 197-215.

CEL (1995). *Prestacion de Servicios de Consultoria para desarrollar Estudios Geocientificos Complementarios en el Campo Geotermico Berlin - Partida 4:Estudio Geovulcanica, y Recursos Geotermicos del Area Berlin-Chinameca. Prefactibilidad Geotermica del Area de Coatepeque. Reconocimiento Geotermico. Informe Definitivo. Internal report (contrado 2301).* Retrieved from San Salvador.

Clift, P., & Vannucchi, P. (2004). Controls on tectonic accretion versus erosion in subduction zones: Implications for the origin and recycling of the continental crust. *Reviews of Geophysics, 42*(2). doi:10.1029/2003RG000127.

Clift, P. D., Chan, L. H., Blusztajn, J., Layne, G. D., Kastner, M., & Kelly, R. K. (2005). Pulsed subduction accretion and tectonic erosion reconstructed since 2.5 Ma from the tephra record offshore Costa Rica. *Geochemistry Geophysics Geosystems*, *6*(9), 1-21. doi:10.1029/2005GC000963.

Damon, P., & Montesinos, E. (1978). Late Cenozoic volcanism and metallogenesis over an active Benioff zone in Chiapas, Mexico. *Arizona Geological Society Digest, 11*, 155-168.

Deligne, N. I., Coles, S. G., & Sparks, R. S. J. (2010). Recurrence rates of large explosive volcanic eruptions. *Journal of Geophysical Research*, *115*. doi:10.1029/2009JB006554.

DeMets, C. (2001). A new estimate for present-day Cocos-Caribbean plate motion: Implications for slip along the Central American volcanic arc. *Geophysical Research Letters*, *28*, 4043-4046.

Donnelly, T. W., Horne, G. S., Finch, R. C., & López-Ramos, E. (1990). Northern Central America: The Maya and Chortis blocks. In J. E. Case & G. Dengo (Eds.), *The Geology of North America: The Caribbean Region* (pp. 37-76). Boulder: The Geological Society of America.

Drexler, J. W., Rose jr., W. I., Sparks, R. S. J., & Ledbetter, M. T. (1980). The Los Chocoyos Ash, Guatemala: A Major Stratigraphic Marker in Middle America and in the Three Ocean Basins. *Quaternary Research*, *13*, 327-345.

Duffield, W. A., Tilling, R. I., & Canul, R. (1984). Geology of El Chichón Volcano, Chiapas, Mexico. *Journal of Volcanology and Geothermal Research*, *20*(1-2), 117-132.

Dull, R. A., Southon, J. R., & Sheets, P. D. (2001). Volcanism, Ecology and Culture: a Reassessment of the Volcán Ilopango TBJ Eruption in the Southern Maya Realm. *Latin American Antiquity, 12*(1), 25-44.

Ehrenborg, J. (1996). A new stratigraphy for the Tertiary volcanic rocks of the Nicaraguan highland. *Geological Society of AmericanBulletin, 108*, 830-842.

Espindola, J. M., Macias, J. L., Tilling, R. I., & Sheridan, M. F. (2000). Volcanic history of El Chichon volcano (Chiapas, Mexico) during the Holocene, and its impact on human activity. *Bulletin of Volcanology, 62*, 90-104.

Feigenson, M. D., & Carr, M. J. (1986). Positively correlated Nd and Sr isotope ratios of lavas from the Central American volcanic front. *Geology, 14*, 79-82.

Feigenson, M. D., Carr, M. J., Maharaj, S. V., Bolge, L. L., & Juliano, S. (2004). Lead isotope composition of Central American Volcanoes: Influence of the Galapagos Plume. *Geochemistry Geophysics Geosystems, 5*(6), 1-14. doi:10.1029/2003GC000621.

Ferrari, L. (2004). Slab detachment control on mafic volcanic pulse and mantle heterogeneity in central Mexico. *Geology, 32*(1), 77-80.

Ferrari, L., López-Martínez, M., Aguirre-Díaz, G., & Carrasco-Núñez, G. (1999). Space-time patterns of Cenozoic arc volcanism in central Mexico: From the Sierra Madre Occidental to the Mexican Volcanic Belt. *Geology, 27*(4), 303-306.

Ferrari, L., Orozco-Esquivel, T., Manea, V., & Manea, M. (2012). The dynamic history of the Trans-Mexican Volcanic Belt and the Mexico subduction zone. *Tectonophysics, 522*, 122-149.

Ferriz, H., & Mahood, G. A. (1984). Eruption rates and compositional trends at Los Humeros volcanic center, Puebla, Mexico. *Journal of Geophysical Research: Solid Earth, 89*(B10), 8511-8524.

Fietzke, J., Liebetrau, V., Günther, D., Gürs, K., Hametner, K., Zumholz, K., . . . Eisenhauer, A. (2008). An alternative data acquisition and evaluation strategy for improved isotope ratio precision using LA-MC-ICP-MS applied to stable and radiogenic strontium isotopes in carbonates. *Journal of Analytical Atomic Spectrometry, 23*(7), 955-961.

Freundt, A., Grevemeyer, I., Rabbel, W., Hansteen, T. H., Hensen, C., Wehrmann, H., . . . Frische, M. (2014). Volatile (H2O, CO2, Cl, S) budget of the Central American subduction zone. *International Journal of Earth Sciences, 103*(7), 2101-2127. doi:10.1007/s00531-014-1001-1.

Freundt, A., Kutterolf, S., Schmincke, H. U., Hansteen, T. H., Wehrmann, H., Perez, W., . . . Navarro, M. (2006). Volcanic hazards in Nicaragua: Past, present, and future. *In:* W. I. Rose, G. J. S. Bluth, M. J. Carr, J. Ewert, L. C. Patino, & J. W. Vallance (Eds.), Volcanic hazards in Central America (Vol. 412, pp. 141-165): *The Geological Society of America Special Publications.*

Funk, J., Mann, P., McIntosh, K., & Stephens, J. (2009). Cenozoic tectonics of the Nicaraguan depression, Nicaragua, and Median Trough, El Salvador, based on seismic-reflection profiling and remote-sensing data. *Geological Society of America Bulletin, 121*(11-12), 1491-1521.

García-Palomo, A., Macías, J., Tolson, G., Valdez, G., & Mora, J. (2002). Volcanic stratigraphy and geological evolution of the Apan region, east-central sector of the Trans-Mexican Volcanic Belt. *Geofisica Internacional Mexico, 41*(2), 133-150.

Gardner, J. E., & Tait, S. (2000). The caldera-forming eruption of Volcan Ceboruco, Mexico. *Bulletin of Volcanology, 62*, 20-33.

Gazel, E., Carr, M., Hoernle, K., Feigenson, M. D., Szymanski, D., Hauff, F., & van den Bogard, P. (2009). Galapagos-OIB signature in southern Central America: Mantle refertilization by arc–hot spot interaction. *Geochemistry Geophysics Geosystems, 10*(2). doi:10.1029/2008GC002246

Grützner, J., Rebesco, M., Cooper, A., Forsberg, C., Kryc, K., & Wefer, G. (2003). Evidence for orbitally controlled size variations of the East Antarctic Ice Sheet during the late Miocene. *Geology, 31*(9), 777-780.

Günther, D., Jackson, S. E., & Longerich, H. P. (1999). Laser ablation and arc/spark solid sample introduction into inductively coupled plasma mass spectrometers. *Spectrochimica Acta Part B: Atomic Spectroscopy, 54*(3), 381-409.

Hannah, R. S., Vogel, T. A., Patino, L. C., Alvarado, G. E., Perez, W., & Smith, D. R. (2002). Origin of silicic volcanic rocks in central Costa Rica: A study of a chemically variable ash-flow sheet in the Tiribi Tuff. *Bulletin of Volcanology, 64*, 117-133.

Herbert, T. D., Lawrence, K. T., Tzanova, A., Peterson, L. C., Caballero-Gill, R., & Kelly, C. S. (2016). Late Miocene global cooling and the rise of modern ecosystems. *Nature Geoscience, 9*(11), 843.

Heydolph, K., Hoernle, K., Hauff, F., Van den Bogaard, P., Portnyagin, M., Bindeman, I., & Garbe-Schönberg, D. (2012). Along and across arc geochemical variations in NW Central America: Evidence for involvement of lithospheric pyroxenite. *Geochimica et Cosmochimica Acta, 84*, 459-491.

Hoernle, K., Abt, D., Fischer, K., Nichols, H., Hauff, F., Abers, G., . . . Strauch, W. (2008). Arc-parallel flow in the mantle wedge beneath Costa Rica and Nicaragua. *Nature, 451*, 1094-1097.

Hoernle, K., van den Bogaard, P., Werner, R., Lissinna, B., Alvarado, G. E., & Garbe-Schönberg, C.-D. (2002). Missing history (16-71 Ma) of the Galapagos hotspot: Implications for the tectonic and biological evolution of the Americas. *Geology, 30*(9), 795-798.

Holbourn, A., Kuhnt, W., Schulz, M., & Erlenkeuser, H. (2005). Impacts of orbital forcing and atmospheric carbon dioxide on Miocene ice-sheet expansion. *Nature, 438*(7067), 483-487.

Hoskuldsson, A., & Robin, C. (1993). Late Pleistocene to Holocene eruptive activity of Pico de Orizaba, eastern Mexico. *Bulletin of volcanology, 55*(8), 571-587.

Hunt, J. B., & Hill, P. G. (2001). Tephrological implications of beam size—sample-size effects in electron microprobe analysis of glass shards. *Journal of Quaternary Science, 16*(2), 105-117.

Jordan, B. R., Sigudsson, H., Carey, S. N., Lundin, S., Rogers, R., Singer, B., & Barguero-Molina, M. (Eds.). (2007b). Petrogenesis of Central American Tertiary ignimbrites and associated Caribbean Sea tephra (Vol. GSA Special papers): *Geological Society of Amercia*.

Jordan, B. R., Sigudsson, H., Carey, S. N., Rogers, R., & Ehrenborg, J. (2006). Geochemical correlation of Caribbean Sea tephra layers with ignimbrites in Central America. In C. Siebe, J. L. Macías, & G. J. Aguirre-Díaz (Eds.), *Neogene-Quaternary Continental Margin Volcanism: A Perspective from México* (Vol. 402, pp. 175-208).

Jordan, B. R., Sigurdsson, H., Carey, S. N., Rogers, R., & Ehrenborg, J. (2007a). Geochemical variation along and across the Central American Miocene paleoarc in Honduras and Nicaragua. *Geochimica et Cosmochimica Acta, 71*, 3581-3591.

Keller, J., Ryan, W. B. F., Ninkovich, D., & Altherr, R. (1978). Explosive volcanic activity in the Mediterranian over the past 200.000 years as recorded in deep-sea sediments. *The Geological Society of America Bulletin, 89*, 591-604.

Kennett, J. P., & Thunell, R. C. (1975). Global increase in Quaternary explosive volcanism. *Science*, 187(4176), 497-502.

Kennett, J. P., McBirney, A. R., & Thunell, R. C. (1977). Episodes of Cenozoic volcanism in the circum-Pacific region. *Journal of Volcanology and Geothemal Research, 2*, 145-163.

Koch, A. J., & McLean, H. (1975). Pleistocene tephra and ash-flow deposits in the volcanic highlands of Guatemala. *The Geological Society of America Bulletin, 86*, 529-541.

Kohn, M. J., & Fremd, T. J. (2008). Miocene tectonics and climate forcing of biodiversity, western United States. *Geology, 36*(10), 783-786.

Kutterolf, S., Freundt, A., & Burkert, C. (2011). Eruptive history and magmatic evolution of the 1.9 kyr Plinian dacitic Chiltepe Tephra from Apoyeque volcano in west-central Nicaragua. *Bulletin of Volcanology, 73*, 811-831. doi: 10.1007/s00445-011-0457-0.

Kutterolf, S., Freundt, A., & Peréz, W. (2008b). The Pacific offshore record of Plinian arc volcanism in Central America, part 2: Tephra volumes and erupted masses. *Geochemistry Geophysics Geosystems, 9*(2), doi:10.1029/2007GC001791.

Kutterolf, S., Freundt, A., Peréz, W., Mörz, T., Schacht, U., Wehrmann, H., & Schmincke, H.-U. (2008a). The Pacific offshore record of Plinian arc volcanism in Central America, part 1: Along-arc correlations. *Geochemistry Geophysics Geosystems, 9*(2), doi:10.1029/2007GC001631.

Kutterolf, S., Freundt, A., Schacht, U., Bürk, D., Harders, R., Mörz, T., & Peréz, W. (2008c). The Pacific offshore record of Plinian arc volcanism in Central America, part 3: Application to forearc geology. *Geochemistry Geophysics Geosystems, 9*(2), doi:10.1029/2007GC001826.

Kutterolf, S., Jegen, M., Mitrovica, J. X., Kwasnitschka, T., Freundt, A., & Huybers, P. (2013). A detection of Milankovitch frequencies in global volcanic activity. *Geology, 41*(2), 227-230. doi:10.1130/G33419.1

Kutterolf, S., Liebetrau, V., Moerz, T., Freundt, A., Hammerich, T., & Garbe-Schönberg, D. (2008d). Lifetime and cyclicity of fluid venting at forearc mound structures determined by tephrostratigraphy and radiometric dating of authigenic carbonates. *Geology, 36*(9), 707-710. doi:10.1130/G24806A.1

Kutterolf, S., Schacht, U., Wehrmann, H., Freundt, A., & Mörz, T. (2007). Onshore to offshore tephrostratigraphy and marine ash layer diagenesis in Central America. In J. Buntschuh & G. E. Alvarado (Eds.), *Central America - Geology, Resources and Hazards* (Vol. 2, pp. 395-423). Lisse, Niederlande, Tokio, Japan: Balkema.

Kutterolf, S., Schindlbeck, J. C., Anselmetti, F. S., Ariztegui, D., Brenner, M., Curtis, J., . . . Wang, K. L. (2016). A 400-ka tephrochronological framework for Central America from Lake Petén Itzá (Guatemala) sediments. *Quaternary Science Reviews, 150*, 200-220. doi:http://dx.doi.org/10.1016/j.quascirev.2016.08.023

Kutterolf, S., Schindlbeck, J. C., Scudder, R. P., Murray, R. W., Pickering, K. T., Freundt, A., . . . Wu, H. (2014). Large volume submarine ignimbrites in the Shikoku Basin: An example for explosive volcanism in the Western Pacific during the Late Miocene. *Geochemistry Geophysics Geosystems, 15*(5), 1837-1851. doi:10.1002/2014gc005263

Kutterolf, S., Schindlbeck, J. C., Robertson, A. H. F., Avery, A., Baxter, A. T., Petronotis, K., & Wang, K. L. (2018). Tephrostratigraphy and Provenance From IODP Expedition 352, Izu-Bonin Arc: Tracing Tephra Sources and Volumes From the Oligocene to Recent. *Geochemistry Geophysics Geosystems, 19*. doi:10.1002/2017GC007100

Kwasnitschka, T. (2009). Volcanic and tectonic development of the Ilopango Caldera, El Salvador: stratigraphic correlation and visulization of emplacement. Diploma tesis, University of Kiel, pp. 157.

Le Maitre, R. W., Streckeisen, A., Zanettin, B., Le Bas, M. J., Bonin, B., Bateman, P., . . . Woolley, A. R. (2002). Igneous Rocks: A Classification and Glossary of Terms. Cambridge, UK: Cambridge University Press.

Ledbetter, M. T. (1985). Tephrochronology of marine tephra adjacent to Central America. *The Geological Society of America Bulletin, 96*, 77-82.

Lenhardt, N., Böhnel, H., Wemmer, K., Torres-Alvarado, I. S., Hornung, J., & Hinderer, M. (2010). Petrology, magnetostratigraphy and geochronology of the Miocene volcaniclastic Tepoztlán Formation: implications for the initiation of the Transmexican Volcanic Belt (Central Mexico). *Bulletin of Volcanology, 72*(7), 817-832.

Lenhardt, N., Hornung, J., Hinderer, M., Böhnel, H., TORRES- ALVARADO, I. S., & Trauth, N. (2011). Build- up and depositional dynamics of an arc front volcaniclastic complex: the Miocene Tepoztlán Formation (Transmexican Volcanic Belt, Central Mexico). *Sedimentology, 58*(3), 785-823.

Macías, J., Arce, J., Mora, J., Espíndola, J., Saucedo, R., & Manetti, P. (2003). A 550- year- old Plinian eruption at El Chichón Volcano, Chiapas, Mexico: Explosive volcanism linked to reheating of the magma reservoir. *Journal of Geophysical Research: Solid Earth, 108*(B12).

Mahood, G. A. (1981). Chemical evolution of a Pleistocene rhyolitic center: Sierra La Primavera, Jalisco, Mexico. *Contributions to Mineralogy and Petrology, 77*, 129-149.

Mahood, G. A., & Halliday, A. N. (1988). Generation of high-silica rhyolite: a Nd, Sr, and O isotopic study of Sierra La Primavera, Mexican Neovolcanic Belt. *Contributions to Mineralogy and Petrology, 100*(2), 183-191.

Mann, C. P., Stix, J., Vallance, J. W., & Richer, M. (2004). Subaqueous intracaldera volcanism, Ilopango Caldera, El Salvador, Cental America. In W. I. Rose, J. J. Bommer, D. L. López, M. J. Carr, & J. J. Major (Eds.), *Natural hazards in El Salvador* (Vol. 375, pp. 159-174). Boulder, Colorado: *The Geological Society of America Special Publications*.

Mann, P., Rogers, R. D., & Gahagan, L. (2007). Overview of plate tectonic history and its unresolved tectonic problems. In: J. Buntschuh & G. E. Alvarado (Eds.), *Central America - Geology, Resources and Hazards* (Vol. 2, pp. 201-238). Lisse, Niederlande, Tokio, Japan: Balkema.

Márquez, A., Oyarzun, R., Doblas, M., & Verma, S. P. (1999). Alkalic (ocean-island basalt type) and calc-alkalic volcanism in the Mexican volcanic belt: A case for plume-related magmatism and propagating rifting at an active margin? *Geology, 27*(1), 51-54.

Mason, B. G., Pyle, D. M., & Oppenheimer, C. (2004a). The size and frequency of the largest explosive eruptions on Earth. *Bulletin of Volcanology, 66*, 735-748.

Mason, B. G., Pyle, D. M., & Oppenheimer, C. (2004b). The size and frequency of the largest explosive eruptions on Earth. *Bulletin of Volcanology, 66*. doi:10.1007/s00445-004-0355-9

Mayer, L., Pisias, N., Kanecek, T., & al., e. (1992). Proceedings of ODP, Initial Reports., 138: College Station, TX (Ocean Drilling Program). doi:10.2973/odp.proc.ir.138.1992.

McGuire, W. J., Howarth, R. J., Firth, C. R., Solow, A. R., Pullen, A. D., Saunders, S. J., . . . Vita-Finzi, C. (1997). Correlation between rate of sea-level change and frequency of explosive volcanism in the Mediterranean. *Nature, 389*, 473-476.

Moore, G., Marone, C., Carmichael, I. S., & Renne, P. (1994). Basaltic volcanism and extension near the intersection of the Sierra Madre volcanic province and the Mexican Volcanic Belt. *Geological Society of America Bulletin, 106*(3), 383-394.

Mora, J., Jaimes-Viera, M., Garduño-Monroy, V., Layer, P., Pompa-Mera, V., & Godinez, M. (2007). Geology and geochemistry characteristics of the Chiapanecan volcanic arc (central area), Chiapas Mexico. *Journal of Volcanology and Geothermal Research, 162*(1), 43-72.

Morán-Zenteno, D. J., Tolson, G., Martınez-Serrano, R., Martiny, B., Schaaf, P., Silva-Romo, G., . . . Solıs-Pichardo, G. (1999). Tertiary arc-magmatism of the Sierra Madre del Sur, Mexico, and its transition to the volcanic activity of the Trans-Mexican Volcanic Belt. *Journal of South American Earth Sciences, 12*(6), 513-535.

Nelson, S. A., & Gonzales-Caver, E. (1992). Geology and K-Ar dating of the Tuxtla Volcanic Field, Veracruz, Mexico. *Bulletin of Volcanology, 55*, 85-96.

Neugebauer, I., Wulf, S., Schwab, M. J., Serb, J., Plessen, B., Appelt, O., & Brauer, A. (2017). Implications of S1 tephra findings in Dead Sea and Tayma palaeolake sediments for marine reservoir age estimation and palaeoclimate synchronisation. *Quaternary Science Reviews, 170*, 269-275.

Newhall, C. G. (1987). Geology of the Lake Atitlàn region, Western Guatemala. *Journal of Volcanology and Geothermal Research, 33*, 23-55.

Newhall, C. G., Paull, C. K., Bradbury, J. P., Higuera-Gundy, A., Poppe, L. J., Self, S., . . . Ziagos, J. (1987). Recent geologic history of Lake Atitlàn, a Caldera Lake in Western Guatemala. *Journal of Volcanology and Geothermal Research, 33*, 81-107.

Newton, A. J., & Metcalfe, S. E. (1999). Tephrochronology of the Toluca Basin, central Mexico. *Quaternary Science Reviews, 18*(8), 1039-1059.

Norman, M., Pearson, N., Sharma, A., & Griffin, W. (1996). Quantitative analysis of trace elements in geological materials by laser ablation ICPMS: instrumental operating conditions and calibration values of NIST glasses. *Geostandards Newsletter*, *20*(2), 247-261.

Nyström, J. O., Levy, B., Troeng, B., Ehrenborg, J., & Carranza, G. (1988). Geochemistry of volcanic rocks in a traverse through Nicaragua. *Revista geologica America Central, 8*, 77-109.

Ortega-Guerrero, B., & Newton, A. J. (1998). Geochemical characterization of Late Pleistocene and Holocene tephra layers from the Basin of Mexico, Central Mexico. *Quaternary Research, 50*(1), 90-106.

Partida, E. G., Rodríguez, V. T., & Birkle, P. (1997). Plio-Pleistocene volcanic history of the Ahuachapan geothermal system, El Salvador: the Concepción de Ataco caldera. *Geothermics, 26*(5-6), 555-575.

Patino, L. C., Carr, M., & Feigenson, M. D. (1997). Cross-arc geochemical variations in volcanic fields in Honduras C.A.: progressive changes in source with distance from the volcanic front. *Contributions to Mineralalogy and Petrology, 129*, 341-351.

Patino, L. C., Carr, M., & Feigenson, M. D. (2000). Local and regional variations in Central American arc lavas controlled by variations in subducted sediment input. *Contributions to Mineralalogy and Petrology, 138*, 256-283.

Plank, T., & Langmuir, C. H. (1988). An evaluation of the global variations in the major element chemistry of arc basalts. *Earth and Planetary Science Letters, 90*, 349-370.

Plank, T., Balzer, V., & Carr, M. (2002). Nicaraguan volcanoes record paleoceanographic changes accompanying closure of the Panama gateway. *Geology, 30*, 1087-1090.

Ponomareva, V., Polyak, L., Portnyagin, M., Abbott, P. M., Zelenin, E., Vakhrameeva, P., & Garbe-Schönberg, D. (2017). Holocene tephra from the Chukchi-Alaskan margin, Arctic Ocean: Implications for sediment chronostratigraphy and volcanic history. *Quaternary Geochronology*, 45, 85-97, https://doi.org/10.1016/j.quageo.2017.11.001.

Ponomareva, V., Portnyagin, M., & Davies, S. M. (2015). Tephra without borders: far-reaching clues into past explosive eruptions. *Frontiers in Earth Science, 3*, 83.

Ponomareva, V., Portnyagin, M., Derkachev, A., Pendea, I. F., Bourgeois, J., Reimer, P. J., . . . Nürnberg, D. (2013). Early Holocene M~ 6 explosive eruption from Plosky volcanic massif (Kamchatka) and its tephra as a link between terrestrial and marine paleoenvironmental records. *International Journal of Earth Sciences, 102*(6), 1673-1699.

Pullinger, C. R. (1998). *Evolution of the Santa Ana volcanic complex,El Salvador*. (MS thesis), Michigan Technological University.

Pyle, D. M. (1995). Mass and energy budgets of explosive volcanic eruptions. *Geophysical Research Letters, 22*. doi:10.1029/95gl00052.

Rabek, K., Ledbetter, M. T., & Williams, D. F. (1985). Tephrochronology of the Western Gulf of Mexico. *Quaternary Research, 23*, 403-416.

Rademacher, M.-R. (2014). *Stratigraphy and depositional processes of the 72 ka old Arce tephra, Coatepeque Caldera (El Salvador). Part 1: Fall out sequence.* (Master Thesis, pp. 103), Christian-Albrechts-Universität zu Kiel, Kiel.

Rampino, M. R., Self, S., & Fairbridge, R. W. (1979). Can Rapid Climatic Change Cause Volcanic Eruptions? *Science, 206*, 826-829. doi:10.1126/science.206.4420.826.

Reynolds, J. H. (1980). Late Tertiary Volcanic Stratigraphy opf Northern Central America. *Bulletin of Volcanology, 43*, 601-607.

Reynolds, J. H. (1987). Timing and sources of Neogene and Quaternary volcanism in South-Central Guatemala. *Journal of Volcanology and Geothermal Research, 33*, 9-22.

Robin, C., & Cantagrel, J. (1982). Le Pico de Orizaba (Mexique): Structure et evolution d'un grand volcán andesitique complexe. *Bulletin volcanologique, 45*(4), 299-315.

Robin, C., Cantagrel, J., & Vincent, P. (1983). Les nuées ardentes de type Saint-Vincent, épisodes remarquables de l'évolution récente du Pico de Orizaba (Mexique). *Bulletin de la Société Géologique de France, 7*(5), 727-736.

Robin, C., Mossand, P., Camus, G., Cantagrel, J.-M., Gourgaud, A., & Vincent, P. M. (1987). Eruptive history of the Colima volcanic complex (Mexico). *Journal of Volcanology and Geothermal Research, 31*(1), 99-113.

Rohr, I. (2014). *Stratigraphy and depositional processes of the 72 ka old Arce tephra, Coatepeque Calder (El Salvador) Part 2: Ignimbrites and fallouts of the upper sequence.* (Master Thesis, pp. 71) Christian-Albrechts-Universität zu Kiel, Kiel.

Rose, W. I., Conway, F. M., Pullinger, C. R., Deino, A., & McIntosh, K. (1999). An improved age framework for late Quaternary silicic eruptions in nothern Central America. *Bulletin of Volcanology, 61*, 106-120.

Rose, W. I., Newhall, C. G., Bornhorst, T. J., & Self, S. (1987). Quaternary silicic pyroclastic deposits of Atitlàn Caldera, Guatemala. *Journal of Volcanology and Geothermal Research, 33*, 57-80.

Rossotti, A., Carrasco-Núñez, G., Rosi, M., & Di Muro, A. (2006). Eruptive dynamics of the "Citlaltépetl pumice" at Citlaltépetl volcano, eastern Mexico. *Journal of Volcanology and Geothermal Research, 158*(3-4), 401-429.

Ryan, W. B. F., Carbotte, S. M., Coplan, J. O., O'Hara, S., Melkonian, A., Arko, R., . . . Zemsky, R. (2009). Global Multi-Resolution Topography synthesis. *Geochemistry Geophysics Geosystems, 10*(3), Q03014. doi:10.1029/2008gc002332.

Schindlbeck, J. C., Kutterolf, S., Freundt, A., Alvarado, G. E., Wang, K. L., Straub, S. M., . . . Woodhead, J. D. (2016a). Late Cenozoic tephrostratigraphy offshore the southern Central American Volcanic Arc: 1. Tephra ages and provenance. *Geochemistry Geophysics Geosystems*. doi:10.1002/2016GC006504.

Schindlbeck, J. C., Kutterolf, S., Freundt, A., Andrews, G., Wang, K.-L., Völker, D., . . . Hoernle, K. (2016c). Alkalic marine tephra layers at ODP Site 1241-Major explosive eruptions from an oceanic volcano in a pre-shield stage? *Journal of Volcanology and Geothermal Research, 328*, 96-104.

Schindlbeck, J. C., Kutterolf, S., Freundt, A., Straub, S., Vannucchi, P., & Alvarado, G. (2016b). Late Cenozoic tephrostratigraphy offshore the southern Central American Volcanic Arc: 2. Implications for magma production rates and subduction erosion. *Geochemistry Geophysics Geosystems, 17*(11), 4585-4604. doi:10.1002/2016GC006503.

Schindlbeck, J. C., Kutterolf, S., Freundt, A., Straub, S. M., Wang, K.-L., Jegen, M., . . . Sandoval, M. I. (2015). The Miocene Galápagos ash layer record of Integrated Ocean Drilling Program Legs 334 and 344: Ocean-island explosive volcanism during plume-ridge interaction. *Geology, 43*(7), 599-602. doi:10.1130/g36645.1

Schindlbeck, J. C., Kutterolf, S., Straub, S. M., Andrews, G. D. M., Wang, K.-L., & Mleneck-Vautravers, M. J. (2018). One Million Years tephra record at IODP Sites U1436 and U1437:

Insights into explosive volcanism from the Japan and Izu arcs. *Island Arc*, e12244. doi:10.1111/iar.12244

Sheth, H. C., Torres-Alvarado, I. S., & Verma, S. P. (2000). Beyond subduction and plumes: A unified tectonic-petrogenetic model for the Mexican volcanic belt. *International Geology Review, 42*(12), 1116-1132.

Siebe, C., Abrams, M., Macías, J. L., & Obenholzner, J. (1996). Repeated volcanic disasters in Prehispanic time at Popocatepetl, central Mexico: Past key to the future? *Geology, 24*(5), 399-402.

Siebert, L., Simkin, T., & Kimberly, P. (2010). *Volcanoes of the world*. Berkeley: University of California Press.

Sieron, K., Capra, L., & Rodríguez-Elizararrás, S. (2014). Hazard assessment at San Martín volcano based on geological record, numerical modeling, and spatial analysis. *Natural hazards, 70*(1), 275-297.

Stoppa, L. (2015). *Tephrachronostratigraphy of the Malpaisillo Caldera (Central-western Nicaragua).* (Master Thesis, pp. 73), Université de Fribourg, Fribourg.

Stoppa, L., Kutterolf, S., Rausch, J., Grobety, B., Pettke, T., Wang, K.-L., & Hemming, S. (2018). The Malpaisillo Formation: A sequence of explosive eruptions in the mid to late Pleistocene (Nicaragua, Central America). *Journal of Volcanology and Geothermal Research*. doi:https://doi.org/10.1016/j.jvolgeores.2018.06.015

Syracuse, E. M., & Abers, G. A. (2006). Global compilation of variations in slab depth beneath arc volcanoes and implications. *Geochemistry, Geophysics, Geosystems, 7*(5), Q05017. doi:10.1029/2005gc001045

van Achterberg, E., Ryan, C. G., Jackson, S. E., & Griffin, W. (2001). LA-ICP-MS in the Earth Sciences - Appendix 3, data reduction software for LA-ICP-MS. *in Sylvester, P.J., ed., Short Course volume 29: St.John's, Mineralogical Association of Canada, p. 239-243.*

Verma, S. P. (2002). Absence of Cocos plate subduction-related basic volcanism in southern Mexico: A unique case on Earth? *Geology, 30*(12), 1095-1098.

Verma, S. P., & Carrasco-Núñez, G. (2003). Reappraisal of the geology and geochemistry of Volcán Zamorano, central Mexico: implications for discriminating the Sierra Madre Occidental and Mexican Volcanic Belt provinces. *International Geology Review, 45*(8), 724-752.

Verma, S. P. (2006). Extension-related origin of magmas from a garnet-bearing source in the Los Tuxtlas volcanic field, Mexico. *International Journal of Earth Sciences, 95*(5), 871.

von Huene, R., Aubouin, J., & al., e. (1985). *Initial Reports DSDP, 84*. Retrieved from Washington, U.S. Government Printing Office.

Walker, J., Mickelson, E., Thomas, R. B., Patino, L. C., Cameron, B., Carr, M. J., . . . Edwards, R. L. (2007). U-series disequilibria in Guatemalan lavas, crustal contamination, and implications for magma genesis along the Central American subduction zone. *Journal of Geophysical Research, 112*(B06205). doi:10.1029/2006JB004589

Watkins, J. S., Moore, J. C., & al., e. (1981). *Initial Reports DSDP, 66*. Retrieved from Washington, U.S. Government Printing Office.

Weyl, R. (1980). Geology of Central America. 2nd Edition, In: Beiträge zur regionalen Geologie der Erden, Bender (Ed.), *Gebr. Borntraeger* (Vol. 15, pp. 371). Berlin - Stuttgart.

Wulf, S., Kraml, M., Brauer, A., Keller, J., & Negendank, J. F. W. (2004). Tephrochronology of the 100 ka lacustrine sediment record of Lago Grande di Monticchio (southern Italy). *Quaternary International, 122*, 7-30.

Table 1. Summary table of major explosive eruptions of El Salvador and Guatemala. Compare with Figure 3.

Volcanic source	Formation	Tephra deposit	Acronym	Age [ka]*	Reference
El Salvador					
Berlin-Pacayal-Volcan Group	Berlin-Chinameca Formation	Old Berlin Tephras 1-5	OBT 1-5		CEL, 1995
		Blanca Rosa Tephra	BRT	75±10; *D*	Kutterolf et al., 2008a
		Twins/A-Tephra	TT/AT	60; *S*	Rohr, 2014
		Pacayal-1 Tephra	PT1	51–53 ka (stratigraphy)	
		Volcan Tephra	VT		
		Pacayal-2 Tephra	PT2		
		Pacayal-3 Tephra	PT3		
St-Vicente-Apastepeque	St-Vicente-Apastepeque Formation	Lower Apastepeque Tephra	LPT		
		Upper Apastepeque Tephra	UPT		
		St. Vicente Tephras 1-4	SVT1-4		
Ilopango Caldera	Ilopango Formation	Old Pumice Ilopango	OPI		Rose et al., 1999
		Terra Blanca 4	TB4	36; *S*	Mann et al., 2004
		Terra Blanca 3	TB3		Kutterolf et al., 2008a
		Terra Blanca 2	TB2		Kwasnitschka, 2009
		Terra Blanca Joven	TBJ	1.6; *D*	Dull et al., 2001
Coatepeque Caldera	Coatepeque-Ataco Formation	Bellavista Tephra	BVT	77±2; *D*	Rose et al., 1999
		Lower and Upper Arce Tephra	L/UACT	72±3; *D*	Kutterolf et al., 2008a
		Congo Tephra	CGT	53±3	
		Conacaste Tephra	CCT	51	
unknown; Coatepeque area	Coatepeque-Ataco Formation	Empalisada Tephra	EPT	350	CEL, 1992
Concepcíon de Ataco Caldera	Coatepeque-Ataco Formation	Chilamatal Ignimbrite	CMT	ca. 406; *S*	Partida et al., 1997
		Ataco Tephras 1-3	AC1-3	ca. 400; *S*	Siebert et al., 2010
					Kutterolf et al., 2016
Guatemala					
Ayarza Caldera	Ayarza Formation	Mixta Fall Tephra	MFT	39; *S*	Kutterolf et al., 2008a
		Piños Altos Tephra	PAT	23; *D*	Petersen and Rose, 1985
		Tapalapa flow	TAT	23; *D*	
Amatitlán Caldera-Antigua	Amatitlán-Antigua Formation	R-Fall Tephra	RFT	>500	Koch and McLean, 1975
		L-Fall Tephra	LFT	191±11; *D*	Rose et al., 1999
		Z1-Z5- Fall Tephras	ZFT	>127; <182 (stratigraphy)	Kutterolf et al., 2008a
		T-Fall Tephra	TFT	119±8; *D*	

		E-Fall Tephra	EFT	51; *S*	
unknown	associated with Amatitlán-Antigua Formation	C-Fall Tephra	CFT	>51; stratigraphy	Kutterolf et al., 2016
Atitlán Caldera	Atitlán-St. Maria Formation	W-Fall Tephra	WFT	158±3; *D*	Rose et al., 1999
		H-Fall Tephra/Los Chocoyos	LCY	84±5; oxygen isotope stratigraphy	Koch and McLean, 1975 Drexler et al., 1980
		I2-I5-Fall Tephras	IFT	>40; stratigraphy	
unknwon	associated Atitlán-St. Maria Formation	X-Fall Tephras	XFT	>119; <158; stratigraphy	Rose et al., 1999
		Y-Fall Tephras	YFT	>119; <158; stratigraphy	
		S-Fall Tephras	SFT	>119; <158; stratigraphy	

Table 2. Summary table of major explosive eruptions of Mexico.

Volcanic source region	Eruptions/ Tephra deposits	Age/Epoch	Reference
<u>Mexico</u>			
Apan region	Matamoros Ignimbrite and pyroclastic flow deposits within the Peñon Andesites	ca. 13 Ma	García -Palomo et al., 2002
	Tecoloquillo Ignimbrite	42-31 ka	
Las Cumbres Volcanic complex including Pico de Orizaba Volcano	several large eruptions	Holocene and Late Pleistocene	Robin and Cantagrel, 1982; Robin et al., 1983; Hoskuldsson and Robin, 1993; Carrasco-Núñez and Rose, 1995; Rossotti et al., 2006
Los Humeros Volcanic Center	Xáltipan Ignimbrite	0.46 Ma	Ferriz and Mahood, 1984
La Malinche Volcano	three explosive eruptions	within the last 40 ka	Siebe et al., 1995
Popocatépetl volcano	numerous eruptions	before 25–20 ka	Siebe et al., 1995, 1996; Boudal and Robin, 1989; Arana-Salinas et al., 2010
	large Plinian eruptions every 3–1 kyr	during the last 20 ka	
Nevado de Toluca Volcano	numerous Plinian eruptions	between ca. 28 and 10 ka	Bloomfield and Valastro, 1974, 1977; Arce et al., 2003, 2005, 2013
Colima Volcano/Colima-Cantaro Chain	several pyroclastic and lava eruptions	tephrostratigraphy < 10 ka	Robin et al., 1987
Sierra La Primavera complex	Tala Tuff	95 ka	Mahood, 1981; Mahood and Halliday, 1988
Cerborucu Volcano	Jala Pumice	ca. 1000 years	Gardner and Tait, 2000
	Marquesado pyroclastic flow	ca. 1000 years	

Table 3. Correlations of 24 tephra layers to well-known eruptions from the CAVA of the last 1.8 Ma that are consecutively numbered from *C1* to *C24*.

	Eruption (Volcanic complex)	**Marine tephra age [Ma]**	**Depth [mbsf]**	**Sample Interval**	**K_2O [wt%]**	**SiO_2 [wt%]**	**MgO [wt%]**	**CaO [wt%]**	**La/Yb**	**Ba/La**	**Ba/Th**	**Rb/Hf**	**Zr/Nb**
C1	TBJ (Ilopango)	<0.001	0.59	**67-499-1R-CC, 0-20 cm**	2.81	77.43	0.20	1.19	7.39	93.20	313.24	17.54	33.37
C2	LAT (Apoyo)	0.023	0.80	**84-569-1H-1, 72-80 cm**	3.01	75.48	0.34	1.68					
C3	TB4 (Ilopango)	0.002 (disturbed)	16.78	**67-499A-3R-2, 78-89 cm**	2.76	76.19	0.27	1.52	7.24	94.70	333.53	16.23	38.65
		0.025	14.70	**67-496-2R-CC, 0-10 cm**	2.70	77.52	0.19	1.16	7.82	90.29	361.99	19.31	25.44
		0.026	5.76	**84-570*-2R-1, 96-103 cm**	2.68	77.13	0.18	1.22	6.87	88.38	351.36	18.42	27.28
		0.035	20.54	**67-496*-3R-3, 54-60 cm**	2.73	77.12	0.19	1.17					
		0.036	21.27	**67-496*-3R-3, 125-131 cm**	2.72	77.14	0.20	1.20	6.76	88.59	320.90	17.79	26.95
		0.036	21.53	**84-568-3H-6, 99-103 cm**	2.72	77.39	0.17	1.13					
C4	MFT (Ayarza)	0.025	14.70	**67-496-2R-CC, 0-10 cm**	4.21	77.26	0.07	0.40	9.45	40.94	104.32	49.59	6.43
		0.037	22.15	**67-496-3R-4,-52-65 cm**	4.09	76.93	0.06	0.42	8.15	41.89	104.22	43.66	7.54
		0.039	8.61	**84-570*-2R-3, 81-86 cm**	4.13	76.99	0.07	0.45	7.38	38.87	92.89	42.99	6.66
		0.048	40.21	**67-496*-5R-2, 6-21 cm**	4.01	77.24	0.06	0.41	5.32	55.97	109.52	52.93	4.88
		0.050	43.05	**67-496-5R-4, 105-120 cm**	4.12	77.23	0.06	0.40	6.24	53.85	110.03	45.09	4.77
		0.036	21.10	**67-496*-3R-3, 110-124 cm**	4.20	76.85	0.07	0.42					
C5	EFT (Amatitlán)	0.050	3.30	**67-498-1H-3, 25-30 cm**	3.64	77.34	0.14	0.90					
		0.047	32.22	**84-568-4H-CC, 5-10 cm**	3.80	77.16	0.14	0.93					
		0.051	44.42	**67-496*-5R-6, 92-97 cm**	4.39	76.06	0.15	0.82	8.74	54.10	121.70	32.21	16.96
C6	CGT (Coatepeque)	0.053	38.75	**84-568-5H-5, 38-45 cm**	4.25	73.34	0.26	1.35	5.59	33.80	69.23	29.70	28.98
		0.053	107.97	**67-499*-13R-4, 53-57 cm**	4.52	73.93	0.17	1.10	6.95	27.97	51.96	28.16	23.85
		0.058	12.68	**67-497*-2R-5, 61-71 cm**	4.42	73.46	0.20	1.33	7.34	38.12	72.07	27.71	26.64
C7	OPT (Berlin-Chinameca)	0.055	40.63	**84-568-5H-6, 83-83 cm**	1.25	57.59	2.21	7.65					
		0.057	108.31	**67-499*-13R-4, 87-92 cm**	1.71	56.69	3.23	7.25	3.93	87.98	461.69	9.47	30.70
C8	IFT (Atitlán)	0.054	1.87	**84-569*-2R-1, 67-68 cm**	3.34	76.08	0.24	1.38					
C9	ACT (Coatepeque)	0.072	109.81	**67-499*-13R-5, 99-112 cm**	4.81	76.06	0.04	0.66	5.62	12.41	23.68	38.10	15.17
C10	LCY (Atitlán)	reworked	7.72	**67-499-2R-5, 67-72 cm**	3.80	77.83	0.11	0.86					
		reworked	7.82	**67-496-2R-1, 32-40 cm**	4.07	77.80	0.08	0.65					
		reworked	5.76	**84-570*-2R-1, 96-103 cm**	4.13	77.83	0.07	0.62					
		0.077	112.61	**67-499*-13R-7, 108-117 cm**	4.14	77.77	0.09	0.64	12.73	77.13	94.21	74.36	6.62
		0.084	5.02	**67-494*-1R-4, 52-54 cm**	4.23	77.97	0.09	0.65	12.84	78.27	97.80	66.79	6.68
		0.081	14.95	**66-487-3R-3, 145-147 cm**	3.92	78.15	0.08	0.63	13.61	67.83	88.76	70.62	8.29
		0.084	116.80	**67-499-14R-2, 30-42 cm**	4.19	77.89	0.09	0.63					
		0.084	51.11	**67-496*-6R-4, 111-126 cm**	4.05	77.80	0.12	0.90	15.79	50.55	74.32	57.95	10.34

		0.084	15.49	**66-487-3R-4, 40-51 cm**	3.84	78.36	0.09	0.65	13.75	75.88	96.84	68.71	6.60
		0.084	3.16	**138-845B-1H-1, 6-9 cm**	4.82	77.39	0.07	0.63					
		0.084	18.27	**67-497*-3R-2, 127-137 cm**	4.15	77.87	0.09	0.67	13.44	70.81	94.53	72.89	7.17
		0.084	41.52	**84-568-5H-7, 15-17 cm**	4.10	78.04	0.09	0.67	13.21	77.22	103.78	82.98	5.94
		0.084	10.32	**84-570*-2R-4, 102-107 cm**	3.80	77.49	0.11	0.79	11.69	83.18	107.30	81.13	6.08
C11	OPI (Ilopango)	0.084	5.02	**67-494*-1R-4, 52-54 cm**	2.75	77.16	0.20	1.29					
C12	OACT (Coatepeque)	0.092	45.98	**84-568*-6R-3, 113-120 cm**	4.00	75.00	0.17	1.13	5.70	86.71	185.41	22.49	37.20
C13	WFT (Atitlán)	0.159	77.03	**67-496*-9R-3, 113-114 cm**	4.72	77.80	0.06	0.65	15.62	34.06	41.16	79.62	5.93
		0.159	37.90	**67-497-5R-2, 120-130 cm**	4.73	77.85	0.07	0.64	14.59	30.35	37.75	84.00	6.36
		0.159	8.73	**84-567*-1R-7, 13-18 cm**	5.04	77.06	0.05	0.68	13.33	32.49	56.17	39.87	8.59
		0.159	81.09	**84-568-10H-1, 97-99 cm**	4.87	77.10	0.12	0.68					
C14	LFT (Amatitlán)	0.191	32.19	**66-487-5R-2, 119-123 cm**	3.67	76.41	0.22	1.37	12.79	43.05	75.75	43.33	15.91
		0.191	7.82	**138-845-B-1H-5, 126-138 cm**	4.09	76.99	0.13	0.79					
		0.191	54.44	**84-570*-6R-6, 77-81 cm**	4.05	76.79	0.13	0.86	12.69	46.69	103.98	40.07	11.91
C15	AOT (Atitlán)	0.306	86.92	**66-488*-11R-1, 42-45 cm**	3.95	77.71	0.08	0.65	10.87	77.12	94.11	75.40	6.44
		0.268	53.29	**66-487-7R-4, 29-35 cm**	3.85	77.68	0.09	0.70	10.24	90.86	154.44	80.24	4.35
		0.306	63.59	**66-487-8R-4, 107-112 cm**	3.65	78.16	0.11	0.80	16.35	48.20	96.88	48.45	11.22
C16	AC3 (Ataco)	0.400	55.81	**67-497*-7R-1, 131-145 cm**	2.96	71.02	0.58	2.53					
C17	TolT (Malpaisillo)	0.420	60.18	**84-570*-7R-3, 118-133 cm**	2.99	72.21	0.43	1.87	3.67	110.09	603.99	14.80	38.47
		0.420	32.97	**67-494-4R-CC, 0-20 cm**	2.99	72.32	0.44	1.88	3.67	136.31	750.61	13.92	31.29
C18	LSabT (Malpaisillo)	0.451	58.32	**67-497-7R-3, 82-87-2 cm**	3.73	74.80	0.30	1.50	3.47	124.88	476.58	12.76	41.73
C19	Feliz (Ilopango)	0.660	22.94	**84-569*-4R-2, 84-86 cm**	3.08	77.39	0.17	1.22	7.64	94.71	299.08	23.36	25.55
C20	UPT (Apastepeque)	0.883	160.63	**67-499-18R-6, 0-25 cm**	3.15	76.65	0.23	1.35	10.05	101.18	311.62	23.76	22.63
C21	Salvamex (Ilopango)	1.025	23.36	**67-495*-3R-3, 136-144 cm**	3.11	77.98	0.19	1.29	10.48	97.11	231.88	25.16	27.15
C22	La Curva (Ilopango)	1.154	40.11	**84-569*-6R-1, 11-14 cm**	3.48	73.06	0.33	1.53	4.19	74.42	258.10	12.22	45.40
C23	LPT (Apastepeque)	1.549	197.19	**67-499-22R-5, 48-52 cm**	3.08	77.63	0.17	1.15	8.98	83.83	211.43	22.29	29.25
C24	LBBP (unknown)	1.843	113.83	**67-494A-9R-1, 33-35 cm**	2.53	75.25	0.33	2.04	4.80	167.35	754.16	16.64	52.44

Table 4. Correlations of 25 tephra layers that were found in multiple marine drill or gravity cores along the arc that are consecutively numbered from *S1* to *S25.*

	correlation to source region along the arc	Age [Ma]	Depth [mbsf]	Sample interval	correlated with tephra layer	K_2O [wt%]	SiO_2 [wt%]	MgO [wt%]	CaO [wt%]	La/Yb	Ba/La	Ba/Th	Rb/Hf	Zr/Nb
S1	Nicaragua	0.10	56.03	**67-496*-7R-1, 103-112 cm**	M66_223, 69-76 cm from Kutterolf et al. (2008a)	1.27	55.96	3.37	7.66	3.95	99.41	543.95	11.03	33.90
S2	Nicaragua	0.16	76.94	**67-496*-9R-3, 104-109 cm**	*s3* (S-CAVA) from Schindlbeck et al. (2016a)	0.92	53.08	4.25	9.41	3.37	101.47	619.56	10.62	36.25
S3	Nicaragua	0.18	78.50	**67-496*-9R-4, 117-143 cm**	170-1039B-3H-3, 92-95 cm from Schindlbeck et al. (2016a)	1.31	56.19	3.33	7.78	3.09	104.58	658.26	10.02	34.07
S4	Nicaragua	0.21	80.32	**67-496*-9R-6, 39-53 cm**	170-1039B-3H-4, 120-123 cm from Schindlbeck et al. (2016a)	0.97	53.43	4.34	9.10	3.08	109.20	689.25	9.52	38.20
S5	Nicaragua	0.39	55.31	**67-497*-7R-1, 81-91 cm**	*s10* (S-CAVA) from Schindlbeck et al. (2016a)	1.72	56.02	3.28	7.61	4.76	58.55	357.56	11.17	37.62
		0.43	93.99	**67-496*-11R-1, 99-106 cm**		1.83	56.34	2.98	7.22	5.37	53.98	323.50	13.01	31.56
		0.42	14.64	**84-569*-3R-3, 51-56 cm**		1.35	57.48	3.16	7.24					
S6	Atitlán	0.51	38.23	**67-494A-1R-1, 108-115 cm**	M66-230, 397 cm from Kutterolf et al. (2008a)	4.23	76.33	0.17	1.21	9.89	55.93	115.76	55.32	9.41
S7	Atitlán	0.54	39.70	**67-494A-1R-2, 70-97 cm**	M66-230, 412-416 cm from Kutterolf et al. (2008a)	3.91	77.61	0.15	0.90					
		0.57	41.40	**67-494A-1R-3, 90-100 cm**		3.99	77.56	0.14	0.83	12.73	48.72	109.76	52.58	8.79
S8	Ilopango	0.60	102.84	**84-568-12H-5, 102-104 cm**		2.46	63.81	1.61	4.12	4.60	53.58	219.07	13.62	37.85
		0.62	96.96	**84-570*-11R-2, 96-99 cm**		2.49	60.55	1.99	5.12	3.68	56.26	207.59	12.80	40.37
S9	Ayarza or Atitlán	1.01	34.95	**84-569*-5R-4, 45-53 cm**	*s21* (S-CAVA) from Schindlbeck et al. (2016a)	4.03	77.96	0.12	0.79	13.85	47.50	106.83	46.53	9.88
S10	Ilopango	1.40	141.57	**84-568* 16R-4, 17-18 cm**		3.30	76.17	0.25	1.42	5.12	99.71	369.67	15.95	31.66
		1.35	102.20	**67-497*-12R-1, 20-23 cm**		2.93	77.11	0.21	1.31	7.74	97.82	332.90	33.14	23.30
S11	Ilopango	1.62	152.71	**84-568*-17R-4, 131-149 cm**		2.99	75.35	0.23	1.39	7.62	95.41	342.33	18.58	34.26
		1.63	169.77	**67-496*-19R-1, 77-82 cm**		3.51	75.69	0.24	1.38	5.11	96.97	366.08	13.38	36.56
		1.67	38.05	**67-495-5R-1, 5-12 cm**		3.55	75.32	0.24	1.25					
		1.65	116.88	**67-497*-13R-5, 93-108 cm**		3.21	75.48	0.27	1.57	7.94	92.99	338.60	18.12	31.46

S12	Ilopango	2.20	191.50	**84-570*-21R-1, 0-12 cm**		3.68	77.35	0.11	0.95	9.58	82.27	219.74	48.48	17.09
		2.29	185.09	**84-568-20H-7, 6-9 cm**		3.76	77.47	0.19	1.10					
S13	Ilopango	2.21	50.44	**67-495*-6R-3, 25-37 cm**		3.74	73.61	0.29	1.25	4.31	64.71	205.02	11.40	49.10
		2.35	214.70	**84-570*-23R-3, 100-105 cm**		3.88	73.37	0.37	1.54	4.79	69.80	190.67	14.30	42.38
S14	Old Coyol Arc	2.26	51.52	**67-495*-6R-3, 133-142 cm**	170-1039B-11H-7, 41-44 cm from Schindlbeck et al. (2016a)	4.23	78.04	0.08	0.86	15.05	48.06	94.53	70.72	10.70
S15	Ilopango	2.89	228.97	**67-496*-25R-4, 6-8 cm**		3.98	68.97	0.67	2.39	4.30	81.69	200.49	13.86	42.63
		3.00	180.96	**67-494A-16R-1, 96-104 cm**		3.77	68.65	0.64	2.15	4.73	99.60	333.86	13.36	41.89
S16	Mexico	4.73	200.64	**84-568*-22R-5, 39-40 cm**		5.14	76.24	0.10	0.68	9.71	48.69	104.11	39.28	14.54
		4.84	189.38	**66-493*-9R-2, 138-144 cm**		5.32	75.72	0.13	0.66	8.24	33.15	66.96	39.83	11.63
		4.73	160.44	**66-492*-18R-4, 21-95 cm**		5.15	75.80	0.13	0.64	9.53	36.70	73.22	34.85	10.84
S17	Coatepeque/Ataco	6.32	134.12	**67-495*-15R-1, 112-115 cm**		4.86	73.91	0.29	1.16	8.81	36.41	89.88	29.47	29.49
		6.30	70.23	**84-569*-9R-2,38-47 cm**		4.75	73.57	0.30	1.20	7.95	36.17	63.36	19.35	26.87
S18	Mexico	8.25	169.50	**66-492*-19R-CC, 0-10 cm**		4.68	76.06	0.14	0.65	9.18	30.49	56.89	34.40	14.71
		8.25	78.59	**84-569*-10R-1, 69-79 cm**		4.47	75.60	0.14	0.91	13.88	35.90	66.52	39.01	13.07
S19	Atitlán	13.82	267.15	**84-567-8R-4, 5-14 cm**		4.75	77.28	0.11	0.75	10.64	57.65	124.56	46.67	14.44
		13.95	249.15	**84-568*-27R-4, 85-94 cm**		5.15	77.32	0.11	0.71	12.36	69.76	125.88	43.89	15.66
S20	Ayarza or Ataco	14.28	267.52	**84-568*-29R-3, 142-150 cm**		4.80	75.58	0.18	0.79	7.79	31.90	66.14	33.18	16.39
		14.54	391.83	**66-493*-30-R-4, 133-136 cm**		4.60	75.96	0.16	0.71					
S21	Atitlán	14.32	269.86	**84-568*-29R-5, 91-105 cm**		4.84	77.32	0.11	0.62	7.83	65.92	104.68	66.79	6.61
		14.32	269.86	**84-568*-29R-5, 91-105 cm**		5.08	77.48	0.06	0.64	8.03	35.72	93.24	29.46	19.23
		14.43	88.15	**84-569*-11R-1, 75-82 cm**		5.19	77.46	0.06	0.61	11.89	48.50	85.50	40.37	11.45
	Coatepeque	14.32	269.86	**84-568*-29R-5, 91-105 cm**		3.87	77.61	0.09	0.82	14.14	10.88	15.52	67.77	6.45
S22	Amatitlán	15.77	352.33	**84-568*-38R-2, 138-148 cm**		4.87	77.53	0.08	0.55	10.74	51.26	92.60	49.37	9.67
		15.88	316.63	**67-496*-34R-4, 63-71 cm**		4.45	77.13	0.06	0.67	6.13	52.10	100.66	26.51	29.12
S23	Coatepeque/Ataco	15.34	192.18	**67-494A-17R-2, 112-118 cm**		5.45	74.33	0.21	0.78	8.86	42.55	73.07	25.75	23.01
		15.90	316.99	**67-496*-34R-4, 99-108 cm**		4.70	74.88	0.16	0.93	6.83	52.10	104.35	28.19	23.72
		16.65	104.59	**84-569*-12R-6, 14-20 cm**		4.68	74.54	0.22	0.86	9.56	38.65	65.90	43.22	21.07

S24	Ilopango	17.02	107.67	**84-569*-13R-1, 97-102 cm**		3.63	76.46	0.18	1.13		47.74	112.30	32.57	17.58
		17.42	199.30	**67-494A-18R-1, 30-33 cm**		3.68	76.85	0.11	1.11					
S25	Amatitlán	21.53	218.69	**84-569*-24R-5, 59-60 cm**		4.81	77.79	0.12	0.75	6.25	56.04	151.39	30.90	13.93
		21.92	209.04	**67-494A-19R-1, 54-62 cm**		4.31	77.46	0.09	0.71					

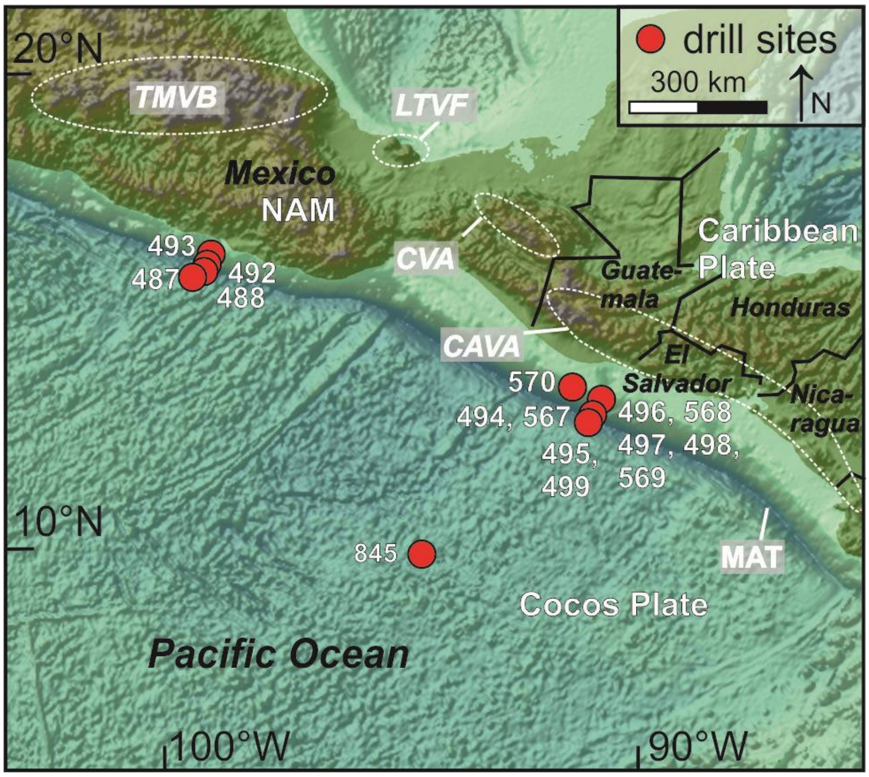

Figure 1. a) Overview map of Central America with the major volcanic regions in southern Mexico, Guatemala and El Salvador. Map created using GeoMapApp (http://www.geomapapp.org; GMRT-Global Multi-Resolution Topography) (Ryan et al., 2009). TMVB= Trans Mexican Volcanic Belt; LTVF= Los Tuxtlas Volcanic Field; CVA= Chiapanecan Volcanic Arc; CAVA= Central American Volcanic Arc; MAT= Middle American Trench; NAM= North American Plate. Red circles indicate drill site positions of deep-sea drilling programs.

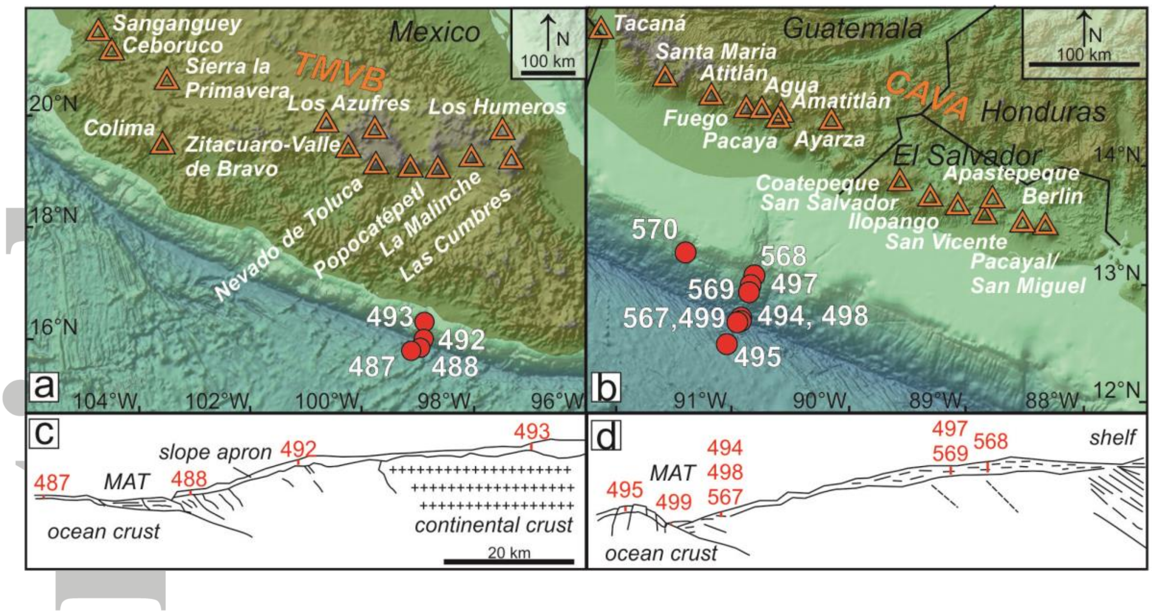

Figure 2. Maps of a) the TMVB in Mexico, and B) the CAVA in Guatemala and El Salvador. Orange triangles mark positions of major Quaternary volcanoes along the arcs. Red circles indicate drill site locations of deep-sea drilling programs. c) and d) Schematic profiles perpendicular to the subduction zone showing sites located on the continental slope and incoming plate offshore Mexico (Sites 487, 488, 492 and 493) and offshore Guatemala (Sites 494-499 and 568-570). MAT= Middle American Trench.

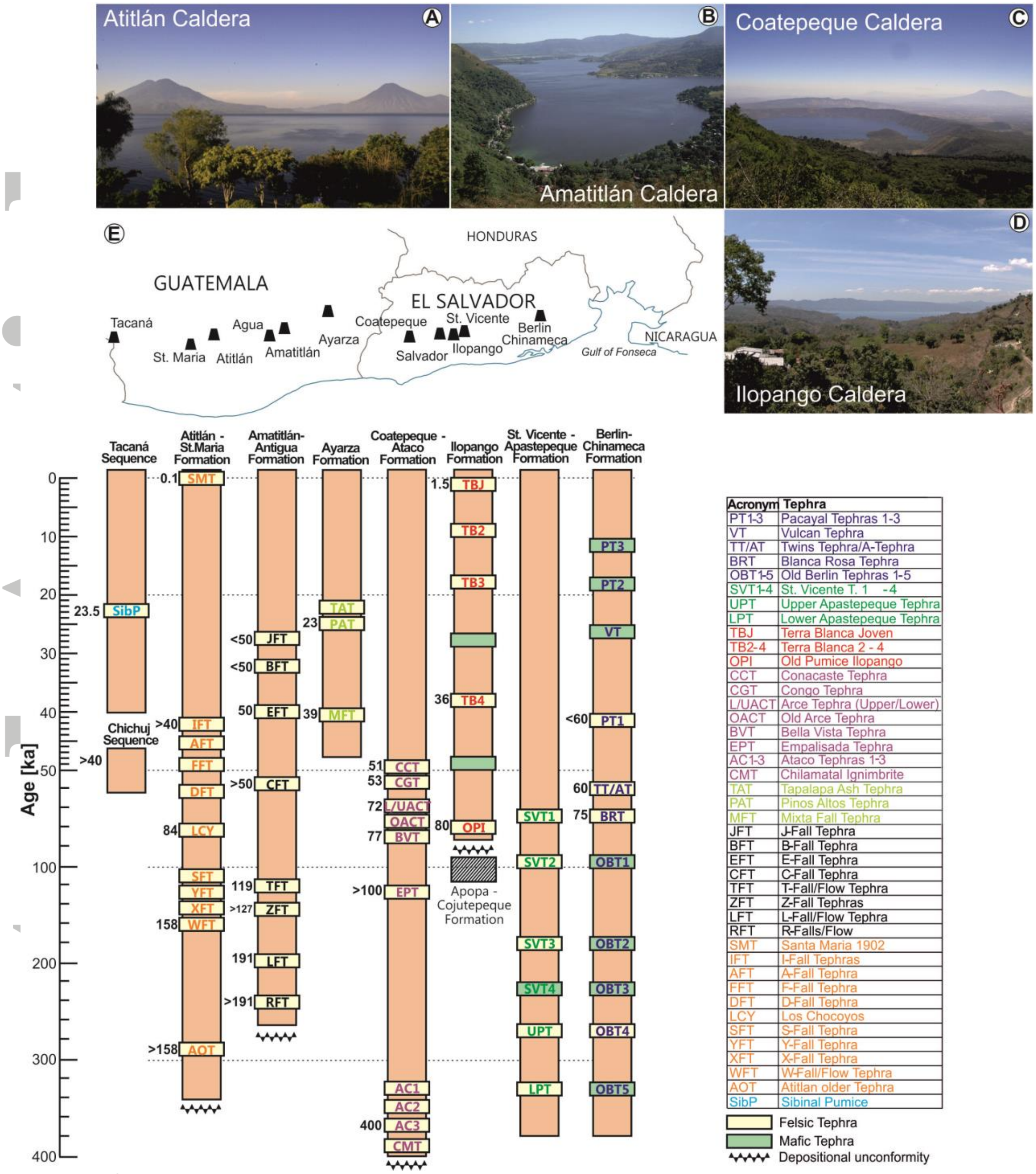

Acronym	Tephra
PT1-3	Pacayal Tephras 1-3
VT	Vulcan Tephra
TT/AT	Twins Tephra/A-Tephra
BRT	Blanca Rosa Tephra
OBT1-5	Old Berlin Tephras 1-5
SVT1-4	St. Vicente T. 1 -4
UPT	Upper Apastepeque Tephra
LPT	Lower Apastepeque Tephra
TBJ	Terra Blanca Joven
TB2-4	Terra Blanca 2 - 4
OPI	Old Pumice Ilopango
CCT	Conacaste Tephra
CGT	Congo Tephra
L/UACT	Arce Tephra (Upper/Lower)
OACT	Old Arce Tephra
BVT	Bella Vista Tephra
EPT	Empalisada Tephra
AC1-3	Ataco Tephras 1-3
CMT	Chilamatal Ignimbrite
TAT	Tapalapa Ash Tephra
PAT	Pinos Altos Tephra
MFT	Mixta Fall Tephra
JFT	J-Fall Tephra
BFT	B-Fall Tephra
EFT	E-Fall Tephra
CFT	C-Fall Tephra
TFT	T-Fall/Flow Tephra
ZFT	Z-Fall Tephras
LFT	L-Fall/Flow Tephra
RFT	R-Falls/Flow
SMT	Santa Maria 1902
IFT	I-Fall Tephras
AFT	A-Fall Tephra
FFT	F-Fall Tephra
DFT	D-Fall Tephra
LCY	Los Chocoyos
SFT	S-Fall Tephra
YFT	Y-Fall Tephra
XFT	X-Fall Tephra
WFT	W-Fall/Flow Tephra
AOT	Atitlan older Tephra
SibP	Sibinal Pumice

☐	Felsic Tephra
🟩	Mafic Tephra
⌃⌃⌃⌃	Depositional unconformity

Figure 3. A) to D) Pictures of large caldera systems in northern Central America. E) Simplified composite stratigraphic successions of known Late Pleistocene/Holocene tephras from highly explosive eruptions in northern Central America (modified from Kutterolf et al., 2008d, 2016) along the northern part of the CAVA; tephra acronyms of respective eruptions are given in the table to the right. Each color represents one formation. Yellow bars mark silicic tephras, and green bars mafic widespread tephras. Major unconformities in the successions are shown by black zigzag bands. Individual numbers next to tephra layers give known eruption ages (Kutterolf et al., 2008b). Tephras without numbers are estimated on the basis of field observations (e.g., thickness of soils and sediments).

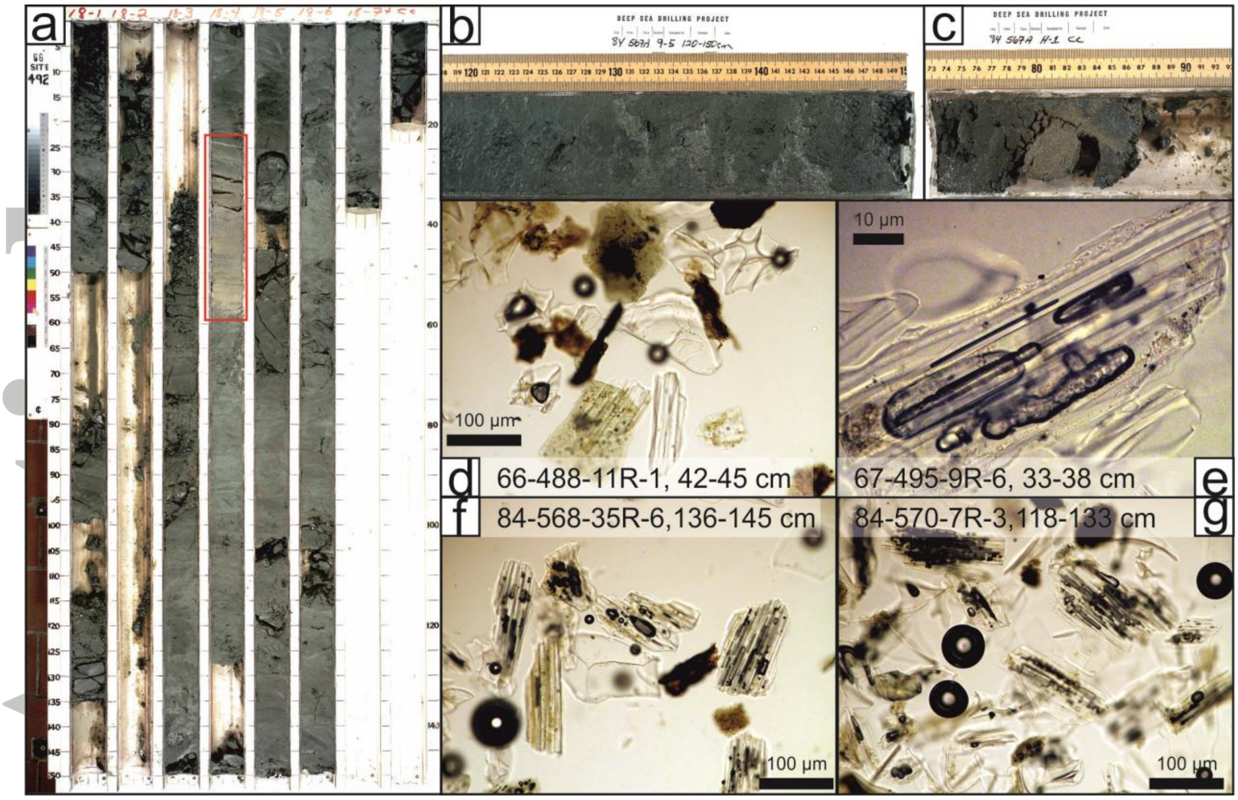

Figure 4. Images of marine drill cores (from www.iodp.tamu.edu) and smear slide pictures of exemplary tephras. a) Highly disturbed core 66-492-18R, drilled offshore Mexico. Red box highlights a thick primary tephra layer that is only slightly disturbed by drilling. b) Biscuited Section 84-567A-9R-5. Lighter patches are remnants of a marine ash layer. c) Core catcher Section 84-567-1R-CC with a brown ash layer. d)-g) Smear slide images of transparent, highly vesicular glass shards. Sample intervals are given in each image.

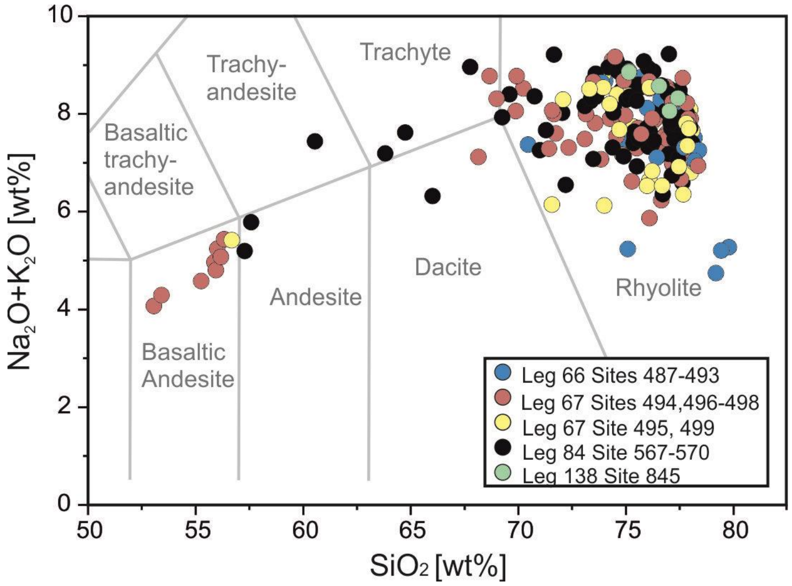

Figure 5. Total alkali versus silica plot to indicate compositional variability in tephras and to discriminate between volcanic rock classes after Le Maitre et al. (2002). Matrix-glass compositional ranges of marine ash beds (normalized to anhydrous compositions). Averages per sample; standard deviation within symbol size.

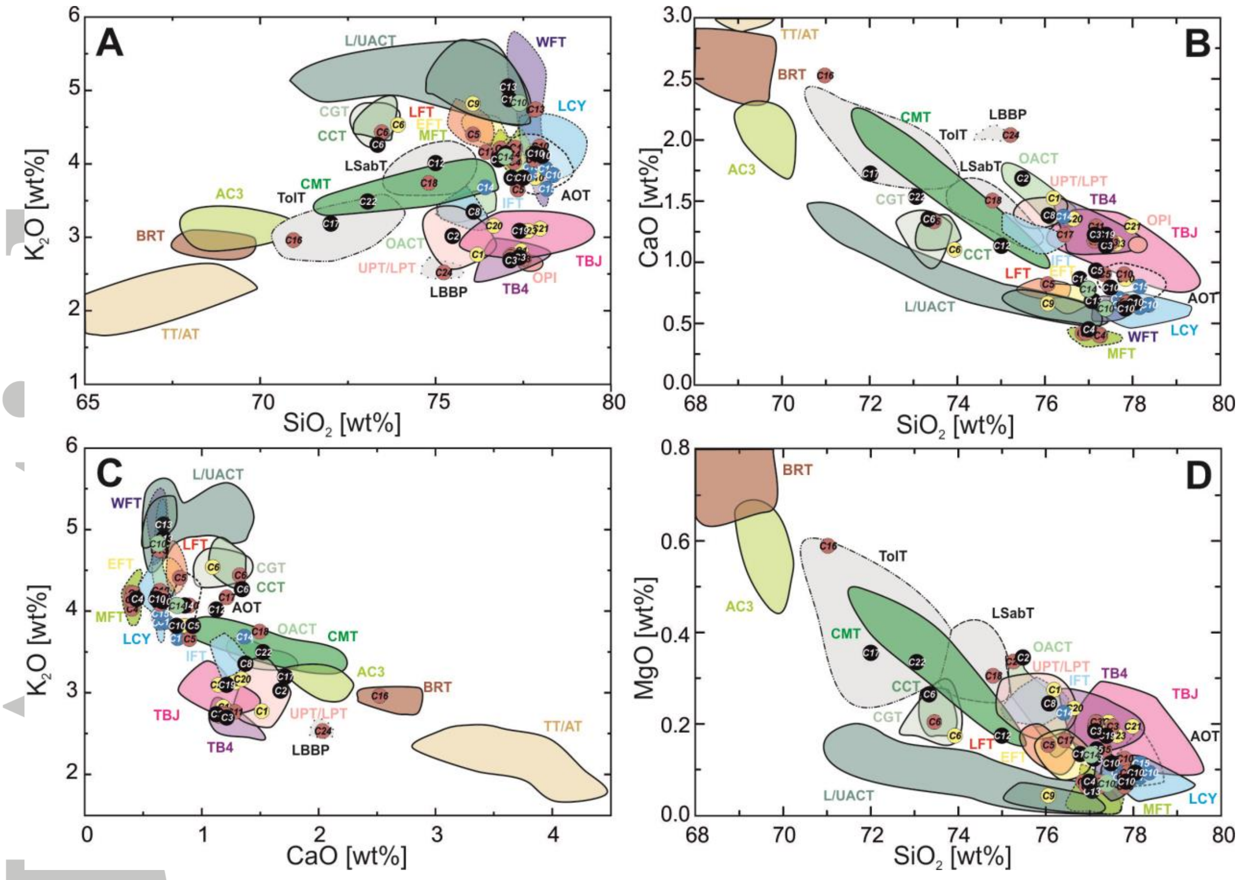

Figure 6. Correlations *C1-C24* to known deposits on land. A to D) Major element glass shard compositions of marine ash beds compared with proximal glass-composition fields of North-CAVA tephras after Kutterolf et al. (2008a, b, c, d, 2016). For clarity, data are averages of all analyses made for each tephra. Color code for marine sites is the same as in Figure 5. Abbreviations of tephra deposits are the same as in Figure 3. Averages per sample; standard deviation within symbol size.

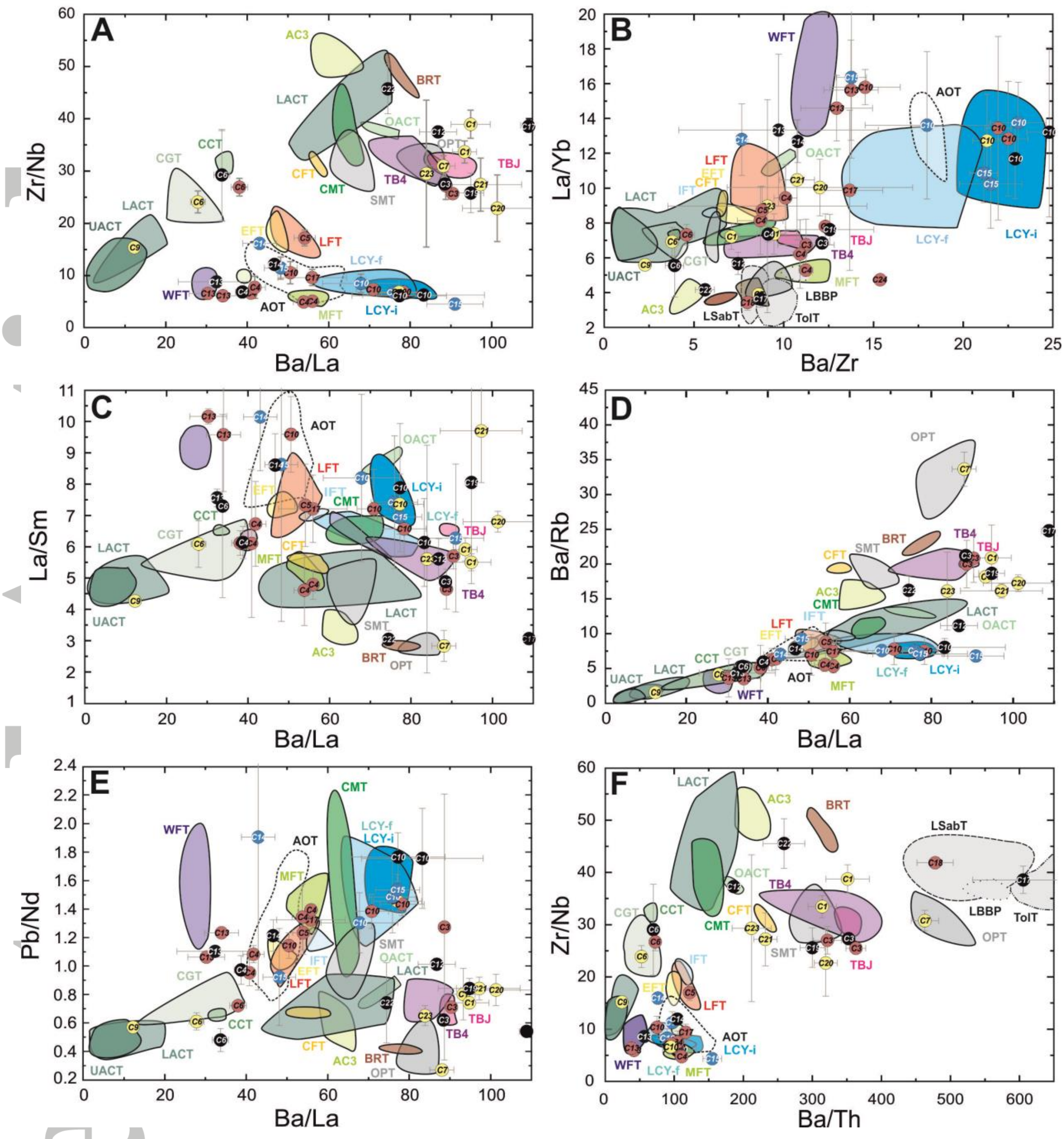

Figure 7. Correlations *C1-C24* to known deposits on land. A to F) Average trace element ratios of glass shard compositions of marine ash layers. Trace element correlation fields for known eruptions from Guatemala and El Salvador after Kutterolf et al. (2008a, 2016). Abbreviations of tephra deposits are the same as in Figure 3. Standard variations per analyzed tephra are shown with gray bars. Color code for marine sites is the same as in Figure 5.

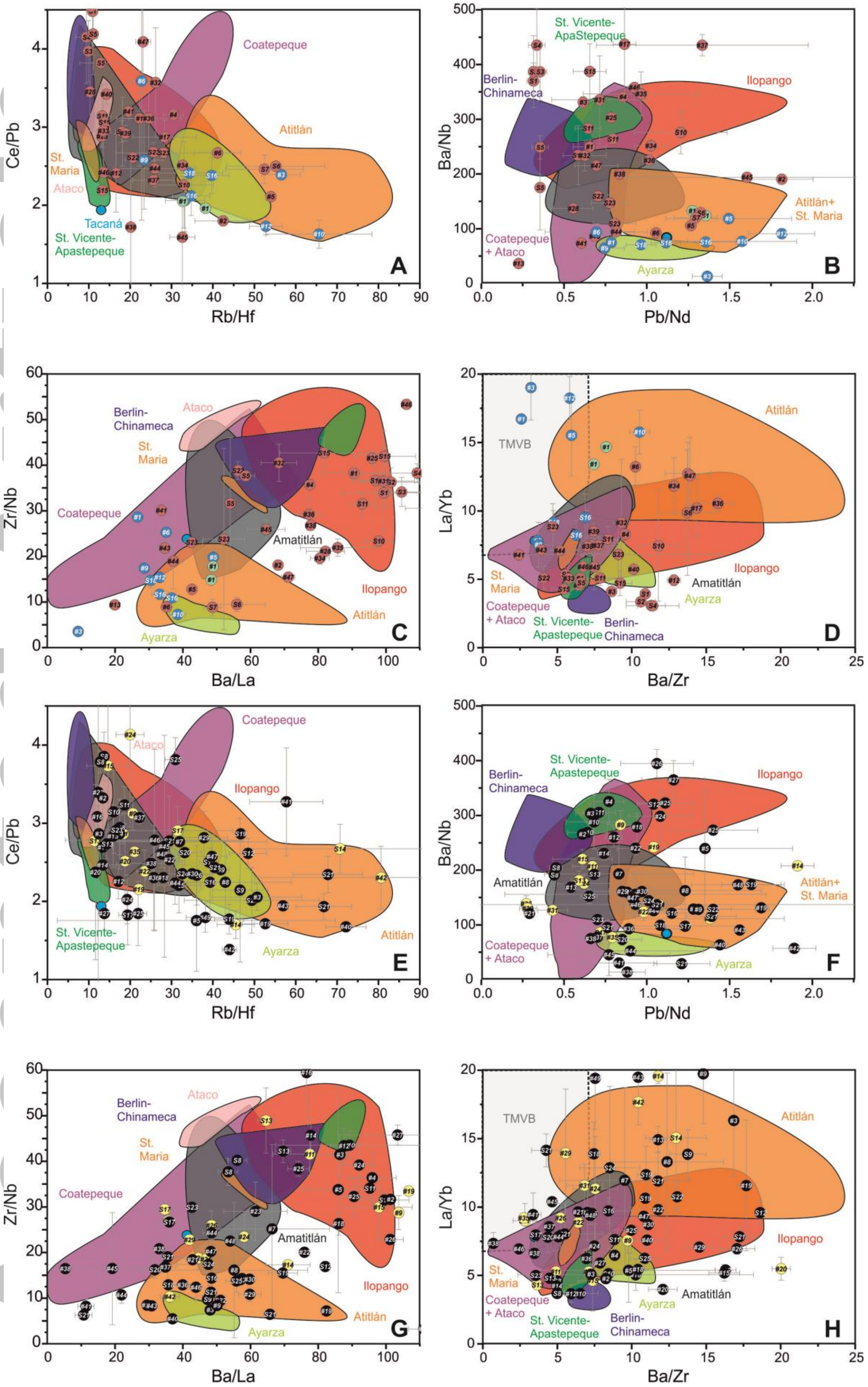
A
Ce/Pb
Rb/Hf
0
10
20
30
40
50
60
70
80
90
1
2
3
4
Coatepeque
Atitlán
St. Maria
Ataco
Tacaná
St. Vicente-Apastepeque
B
Ba/Nb
Pb/Nd
0.0
0.5
1.0
1.5
2.0
0
100
200
300
400
500
St. Vicente-ApaStepeque
Berlin-Chinameca
Ilopango
Atitlán+ St. Maria
Coatepeque + Ataco
Ayarza
C
Zr/Nb
Ba/La
0
20
40
60
80
100
0
10
20
30
40
50
60
Berlin-Chinameca
Ataco
St. Maria
Coatepeque
Amatitlán
Ilopango
Atitlán
Ayarza
D
La/Yb
Ba/Zr
0
5
10
15
20
25
TMVB
Atitlán
Ilopango
Amatitlán
Ayarza
St. Maria
Coatepeque + Ataco
St. Vicente-Apastepeque
Berlin-Chinameca
E
Ce/Pb
Rb/Hf
Coatepeque
Ataco
Ilopango
Atitlán
Ayarza
St. Vicente-Apastepeque
F
Ba/Nb
Pb/Nd
Berlin-Chinameca
St. Vicente-Apastepeque
Ilopango
Amatitlán
Atitlán+ St. Maria
Coatepeque + Ataco
Ayarza
G
Zr/Nb
Ba/La
Berlin-Chinameca
Ataco
St. Maria
Coatepeque
Amatitlán
Ilopango
Atitlán
Ayarza
H
La/Yb
Ba/Zr
TMVB
Atitlán
Ilopango
St. Maria
Coatepeque + Ataco
Ayarza
Amatitlán
St. Vicente-Apastepeque
Berlin-Chinameca

Figure 8. Correlations of site-to-site correlations (*S1*-*S25*) and all remaining single ash beds (#) to volcanic complexes of Guatemala and El Salvador. Trace element ratios of glass shard compositions. A-D) Marine tephras of Sites 487, 488, 492 and 493 offshore Mexico, and incoming plate Sites 495 and 499 offshore Guatemala. E-H) Marine tephras from slope Sites 567, 568, 569 and 570. Standard variations per analyzed tephra are shown with gray bars. Color code for marine sites is the same as in Figure 5.

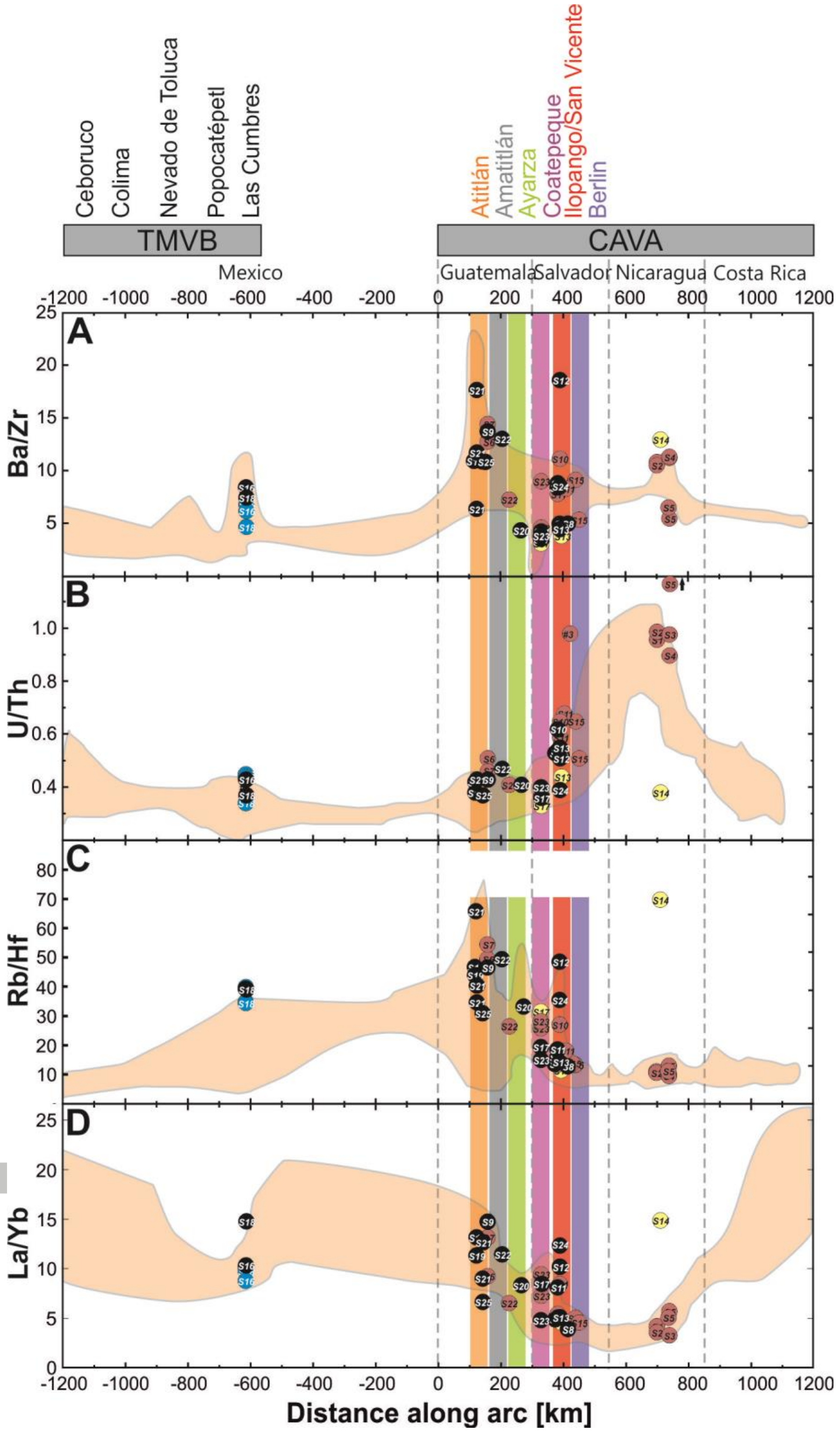

Figure 9. Comparison of average glass compositions of marine ash layers that can be correlated between several sites (*S1*-*S25*) with Ba/Zr, U/Th, Rb/Hf, and La/Yb variations along the CAVA and Mexican arcs as discussed in the text. Modified after Kutterolf et al. (2016). Along-arc variations of CAVA are based on corresponding felsic and mafic ratios as well as glass and bulk rock compositions (Kutterolf et al., 2015; Carr et al., 2007). Mexican compositional fields are only based on bulk rock data, given in Luhr et al. (2006), but are assumed to provide the same provenance information. Positive distances along the arc

represent CAVA provenances; Negative distances along the arc indicate Mexican origin. Color code for marine sites is the same as in Figure 5.

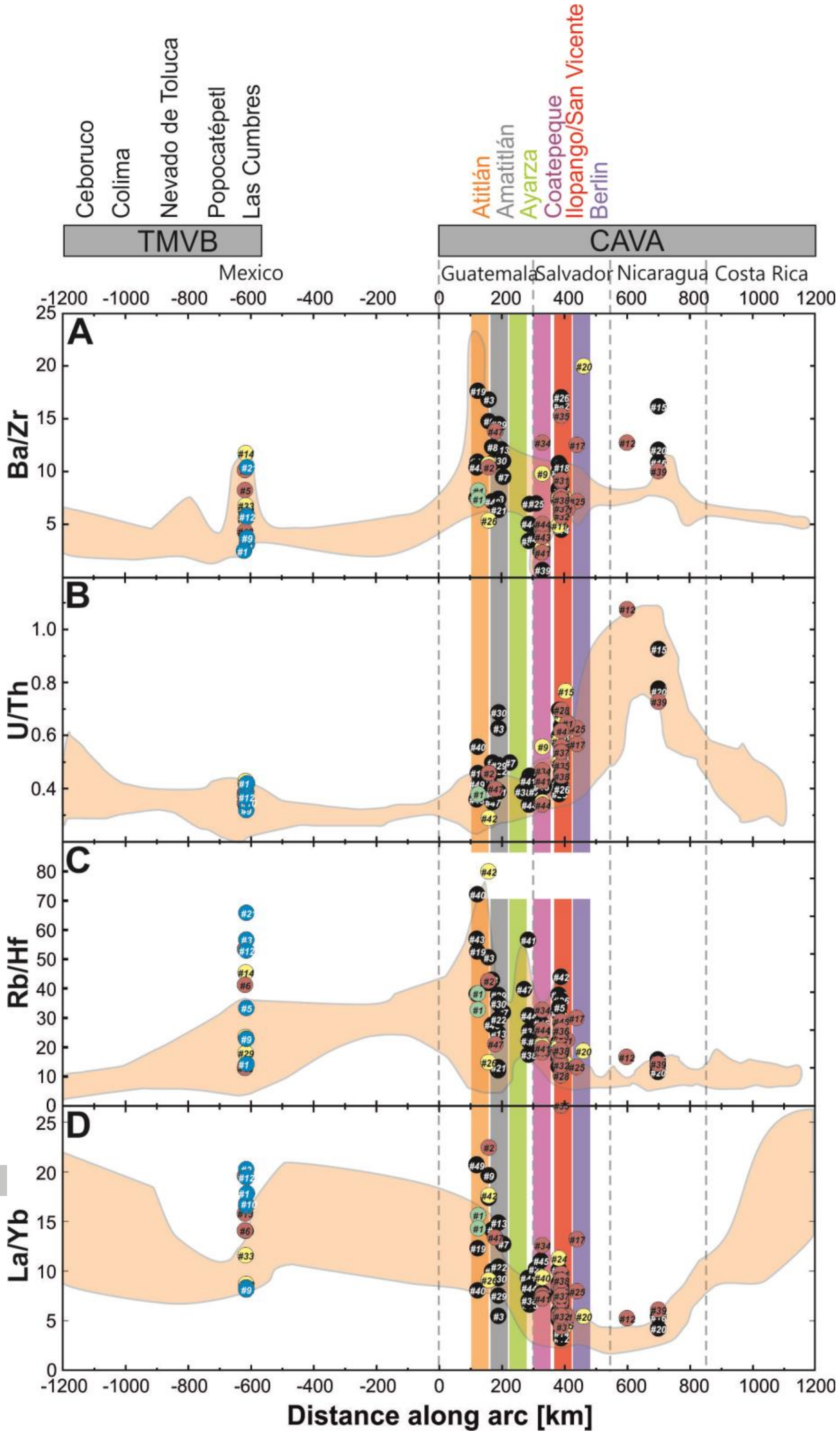

Figure 10. Comparison of average glass compositions of single marine ash beds (#x) with Ba/Zr, U/Th, Rb/Hf, and La/Yb variations along the CAVA and Mexican arcs as discussed in the text. Modified after Kutterolf et al. (2016). For further information see Fig. 9. Color code for marine sites is the same as in Figure 5.

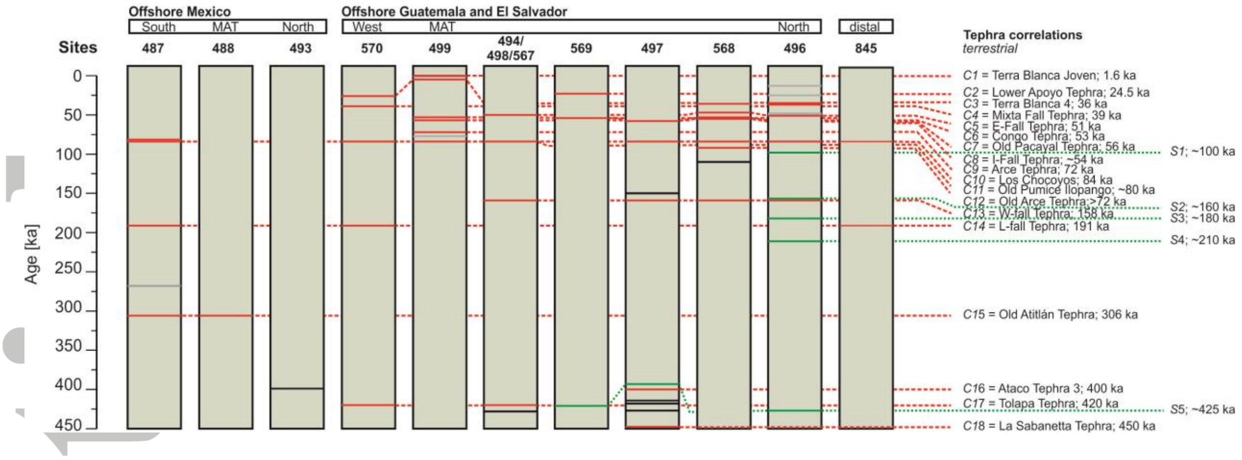

Figure 11. Compositionally correlated tephra layers of the last 450 ka. Tephra layers *C1* through *C18* provide chronostratigraphic links between the drill sites offshore northern CAVA and Mexico. Sites are arranged from South (right) to North (left) offshore Mexico and from West to North offshore Guatemala and El Salvador. Site 845 is more distal (~600 km) offshore Guatemala. Layers *C1* to *C18* (red) correlate with specific tephras on land as shown in Figures 6 and 7 and Table 3. Layers *S1–S5* (green) are correlated between the sites and to source regions on land (see Table 4). Unlabeled ash beds could not be correlated between sites or to known eruptions on land (black).

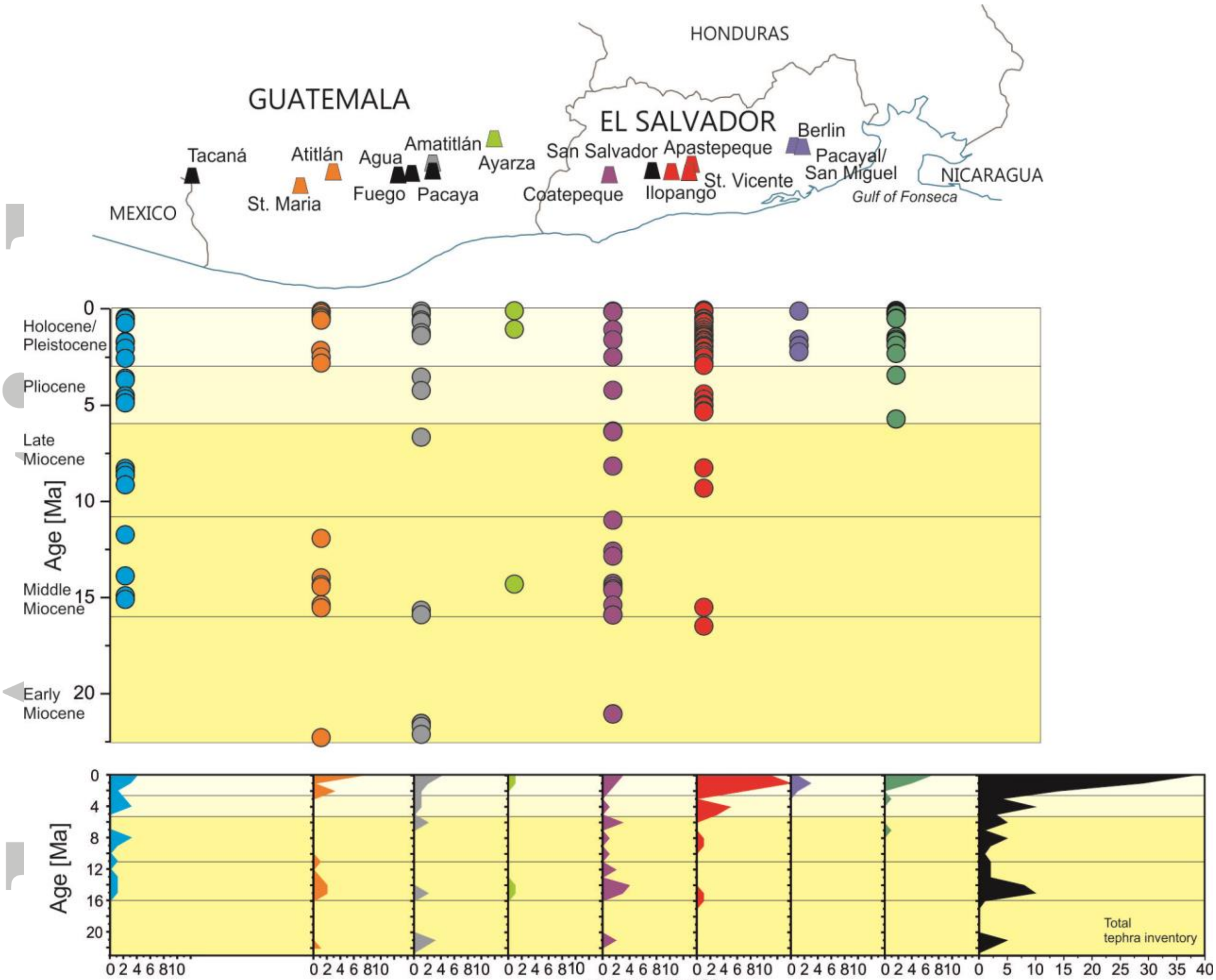

Figure 12. Distribution of marine tephra layers along the arcs over time. a) Each colored circle represents a single eruptive event from the respective volcanic complex along the arcs; color code matches the colored major volcanic edifices in the upper panel; blue and dark green represents an origin from Mexico or Nicaragua, respectively. b) Average number of tephras/eruptions per 1 Myr window to highlight episodes of increased explosive volcanic activity; the color code represents the volcanic complexes/arc segments like in panel a). The black curve represents the total tephra inventory.

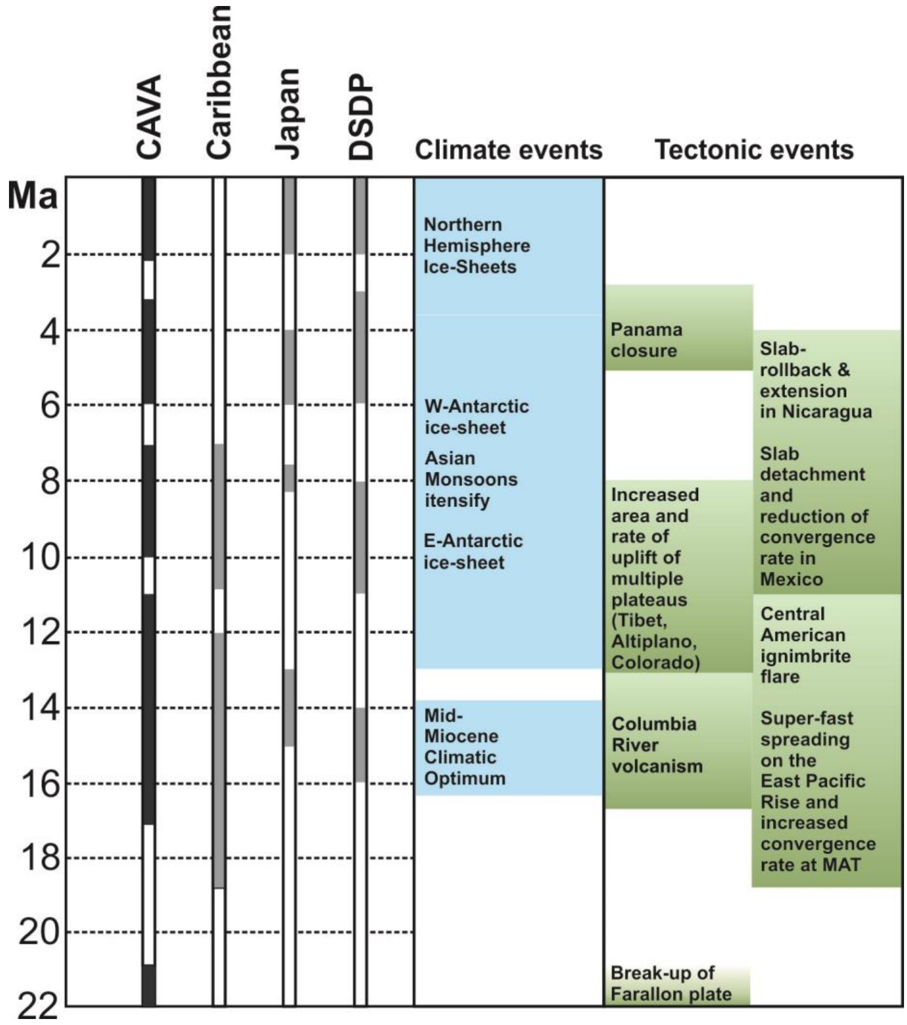

Figure 13. The temporal relationship of Neogene and Quaternary episodes of high volcanic activity and tectonic and climatic events. Episodes of increased volcanism of Central America (CAVA) from this study. Caribbean data from Sigurdsson et al. (2000) and Carey and Sigurdsson (2000). Episodes of increased volcanism of Japan after Mahony et al. (2016). Data compilation of the SW Pacific, Central America, Cascades after Kennet et al. (1977). Climatic and tectonic events after Zachos et al. (2001), Rogers et al. (2002), Mann et al. (2007) and Ferrari (2004).